AFRL-RH-WP-TR-2023-0051

EXPOSURE TO NON-STEADY-STATE OXYGEN IS REFLECTED IN CHANGES TO ARTERIAL BLOOD GAS VALUES, PREFRONTAL CORTICAL ACTIVITY, AND SYSTEMIC CYTOKINE LEVELS

Elizabeth G. Damato, Seth J. Fillioe, Lily K. Norton, Alireza Abdollahifar, Michael J. Decker
Department of Physiology & Biophysics

Joseph J. Piktel
Department of Emergency Medicine

Seunghee P. Margevicius
Department of Population & Quantitative Health Sciences

Kingman P. Strohl
Department of Pulmonary

David S. Burch
711 HPW/RHBF

September 2023
Final Report

AIR FORCE RESEARCH LABORATORY
711TH HUMAN PERFORMANCE WING,
AIRMAN SYSTEMS DIRECTORATE,
WRIGHT-PATTERSON AFB, OH 45433
AIR FORCE MATERIEL COMMAND
UNITED STATES AIR FORCE

NOTICE AND SIGNATURE PAGE

Using Government drawings, specifications, or other data included in this document for any purpose other than Government procurement does not in any way obligate the U.S. Government. The fact that the Government formulated or supplied the drawings, specifications, or other data does not license the holder or any other person or corporation; or convey any rights or permission to manufacture, use, or sell any patented invention that may relate to them.

This report was cleared for public release by the Air Force Research Laboratory Public Affairs Office and is available to the general public, including foreign nationals. Copies may be obtained from the Defense Technical Information Center (DTIC) (http://www.dtic.mil).

AFRL-RH-WP-TR-2023-0051 HAS BEEN REVIEWED AND IS APPROVED FOR PUBLICATION IN ACCORDANCE WITH ASSIGNED DISTRIBUTION STATEMENT.

BURCH.DAVID.S.1503870319 Digitally signed by BURCH.DAVID.S.1503870319 Date: 2023.10.10 12:06:58 -04'00'

DAVID S. BURCH, DR-III, PhD
Senior Biomedical Engineer
Principal Investigator & Technical Lead
Biomedical Impact of Flight Branch
Air & Space Biosciences Division

HART.COREY.RICHARD.1467934097 Digitally signed by HART.COREY.RICHARD.1467934097 Date: 2023.10.13 08:31:47 -04'00'

COREY R. HART, DR-III, PhD
Core Research Area Lead
Biomedical Impact of Air & Space
Biomedical Impact of Flight Branch
Air & Space Biosciences Division

This report is published in the interest of scientific and technical information exchange, and its publication does not constitute the Government's approval or disapproval of its ideas or findings.

REPORT DOCUMENTATION PAGE

Form Approved
OMB No. 0704-0188

1. REPORT DATE *(DD-MM-YY)*	2. REPORT TYPE	3. DATES COVERED *(From - To)*
22-04-23	Final	June 2019 – March 2023

4. TITLE AND SUBTITLE

Exposure to Non-Steady-State Oxygen is Reflected in Changes to Arterial Blood Gas Values, Prefrontal Cortical Activity, and Systemic Cytokine Levels

5a. CONTRACT NUMBER
FA8650-19-C-6103

5b. GRANT NUMBER

5c. PROGRAM ELEMENT NUMBER
62202F

6. AUTHOR(S)
Elizabeth G. Damato[1], Joseph S. Piktel[2], Seunghee P. Margevicius[3], Seth J. Fillioe[4†], Lily K. Norton[5†], Alireza Abdollahifar[1], Kingman P. Strohl[1], David S. Burch[6], Michael J. Decker[1]

5d. PROJECT NUMBER

5e. TASK NUMBER

5f. WORK UNIT NUMBER
H0ZE

7. PERFORMING ORGANIZATION NAME(S) AND ADDRESS(ES)
1. Department of Physiology & Biophysics, Center for Aerospace Physiology, School of Medicine, Case Western Reserve University, Cleveland, OH
2. Department of Emergency Medicine, Metrohealth Medical Center, Case Western Reserve University School of Medicine, Cleveland, OH
3. Department of Population and Quantitative Health Sciences, Case Western Reserve University School of Medicine, Cleveland, OH
4. Cuyahoga Community College, Cleveland, OH
5. Jacobs School of Medicine and Biomedical Sciences, University at Buffalo, Buffalo NY
† Formerly of the Department of Physiology & Biophysics, School of Medicine, Case Western Reserve University, Cleveland, OH

8. PERFORMING ORGANIZATION REPORT NUMBER

9. SPONSORING/MONITORING AGENCY NAME(S) AND ADDRESS(ES)
6Air Force Materiel Command
Air Force Research Laboratory
711th Human Performance Wing
Airman Systems Directorate
Airman Biosciences Division
Biomedical Impact of Flight Branch
Wright-Patterson AFB, OH 45433

10. SPONSORING/MONITORING AGENCY ACRONYM(S)
711 HPW/RHBC

11. SPONSORING/MONITORING AGENCY REPORT NUMBER(S)
AFRL-RH-WP-TR-2023-0051

12. DISTRIBUTION/AVAILABILITY STATEMENT
Distribution Statement A: Approved for public release.

13. SUPPLEMENTARY NOTES
Report contains color. AFRL-2023-4861, cleared 2 October 2023

14. ABSTRACT

Onboard oxygen generating systems (OBOGS) provide increased inspired oxygen (F_iO_2) to mitigate risk of neurologic injury within high altitude aviators. When operating in the 'Normal' mode, OBOGS delivers highly variable oxygen concentrations that may oscillate around a predetermined F_iO_2 set point, even when the aircraft cabin altitude is relatively stable. Steady-state exposure to 100% F_iO_2 evokes neurovascular vasoconstriction, diminished cerebral perfusion, and altered electroencephalographic (EEG) activity. Whether non-steady state F_iO_2 exposure leads to similar outcomes is unknown. This study's objective was to characterize physiologic responses to both steady state and non-steady state F_iO_2 exposure during normobaric and hypobaric environmental pressures emulating cockpit pressures within tactical aircraft.

15. SUBJECT TERMS
Hypobaric, oxygen, arterial, brain, neurovascular, functional spectroscopy

16. SECURITY CLASSIFICATION OF:			17. LIMITATION OF ABSTRACT:	18. NUMBER OF PAGES	19a. NAME OF RESPONSIBLE PERSON (Monitor)
a. REPORT	b. ABSTRACT	c. THIS PAGE			Amy McKleroy
Unclassified	Unclassified	Unclassified	SAR	36	19b. TELEPHONE NUMBER *(Include Area Code)* N/A

SF298: Additional block 14 info

Methods: Participants received an indwelling radial arterial catheter, were seated in a hypobaric chamber and attached to a system providing steady-state F_iO_2 or non-steady state F_iO_2 levels oscillating ± 15% of prescribed set points. Exposure to steady-state and non-steady state F_iO_2 occurred at normobaric (749 millimeters of mercury (mmHg)) and hypobaric (565 mmHg and 494 mmHg) environmental conditions. An arterial blood gas (ABG) sample was obtained after each series of F_iO_2 oscillations, and again during steady-state F_iO_2. Continuous functional near-infrared spectroscopy (fNIRS) quantified prefrontal cortical activity levels during cognitive testing following each sequence of non-steady state F_iO_2 exposures. Blood serum samples were also obtained to determine levels of multiple systemic markers suggestive of physiological stress prior to, and again following the experimental exposure.

Results: Steady state exposure to 21% F_iO_2 during normobaria produced ABG values within anticipated ranges. Exposure to non-steady state F_iO_2 led to P_aO_2 levels that were higher upon cessation of non-steady state F_iO_2 than when measured 120 seconds later during steady state exposure to the same F_iO_2 level. This pattern was consistent across all F_iO_2 ranges, and at each of the three barometric pressure conditions. Prefrontal cortical activation during cognitive testing was significantly lower following exposure to non-steady state $F_iO_2 > 50\%$ and $< 100\%$ during both normobaria (749 mmHg) and hypobaria of 494 mmHg. Serum analyte levels (IL-6, IP-10, MCP-1, MDC, IL-15, and VEGF-D) were increased 48 hours following exposure to both increased F_iO_2 and hypobaria.

Discussion: Exposure to non-steady state F_iO_2 levels > 50% led to reduced levels of prefrontal cortical brain activation during a cognitive challenge. This is consistent with an evoked pattern of neurovascular constriction and dilation, with ebbs and flows in prefrontal cortical perfusion. Whether reduced perfusion deteriorated cognitive performance is yet to be determined. In addition, the mechanism leading to increased systemic levels of proinflammatory serum analytes remains unclear.

TABLE OF CONTENTS

1.0 INTRODUCTION

Hypobaric hypoxia and decompression injury are among the risks awaiting tactical aviators within their austere, high altitude environment. Life support equipment providing a continuous fraction of inspired oxygen (F_iO_2), typically between 35-100 percent (%), is an intended neuroprotection against those hazards. Exposure to enhanced oxygen concentrations also convey a risk. Prolonged exposure is pathologic to multiple organ systems *(Asfar et al., 2015;Brugniaux et al., 2018)* while short term exposures reduce cerebral perfusion and alters cortical electroencephalographic activity *(Damato et al., 2020)*.

The original technology to provide increased F_iO_2 levels, necessary to survive within high altitude environments, was first implemented during World War I. Those systems used liquid oxygen, a relatively simple approach *(Griffiths, 1922; Grayson-Smith and Findlay, 1946)*. As the liquid oxygen transitioned into a gaseous state it flowed into the aircrew breathing system. There, it was diluted with air to deliver a specific level of F_iO_2 to the aviator, with that level determined by cockpit ambient pressure *(Elliott and Schmitt, 2019)*. Further dilution of the F_iO_2 could occur within the gas regulators, such as that found within diluter demand masks. The success of liquid oxygen systems led to further development and, beginning in the early 1940s, the installation of a small refillable liquid oxygen container within almost every tactical aircraft. The simplicity of liquid oxygen systems contributes to their continued use.

Onboard oxygen generation systems (OBOGs) began replacing liquid oxygen-based life support systems during the 1970s *(Manatt, 1981)*. Their operation is dependent upon a stream of ambient air being forced through a molecular sieve. Only oxygen molecules pass through the sieve and into a series of small storage tanks *(Bhat et al., 2017)*. Upon release from the storage tanks, dilution occurs in diluter-demand regulators. The criteria of both minimum and maximum F_iO_2 delivered are determined according to the aircraft cockpit pressure. The OBOGs typically incorporate "safety pressure," which is continuous positive pressure within the pilot's mask, of 1.25 - 4 centimeters of water (cmH_2O). Systems without safety pressure, or when safety pressure is turned off will provide 0-0.5 cmH_2O pressure within the mask. In contrast with liquid oxygen systems that deliver a relatively constant F_iO_2 concentration into the life support system, the F_iO_2 delivery from the OBOGs system follows a sinusoidal pattern *(Elliott and Schmitt, 2019)*.

Oxygen-induced reductions in cerebral perfusion, and subsequently, oxygen delivery to the brain, was first characterized in healthy humans with indwelling arterial and venous catheters by Lambertsen et al., in 1953 *(Lambertsen et al., 1953)*. Those findings have since been replicated using noninvasive techniques *(Floyd et al., 2003; Mattos et al., 2019)*, which more recent studies revealing that reductions in cerebral perfusion begin during exposure to an F_iO_2 of 60% *(Damato et al., 2022)*. Inspired oxygen levels > 60% not only influence neurovascular tone, systemic sequelae can range from decreased cardiac output *(Lodato, 1989)* and onset of lung alveolar collapse and atelectasis *(Dussault et al., 2016)*, to tonic clonic seizure activity when hyperoxia occurs during hyperbaric conditions *(Ciarlone et al., 2019)*.

In contrast with well characterized neuro- and physiological outcomes of exposure to steady state F_iO_2, fewer studies have focused upon outcomes of exposure to non-steady state F_iO_2. Those findings, often derived from cell *(Tiboldi et al., 2022)*, rodent, or swine models *(Boehme et al., 2019)* reveal inflammation of pulmonary epithelium. Those observations concur with studies by Formenti et al. *(Formenti et al., 2017;Formenti and Farmery, 2017)* revealing that non-steady state F_iO_2 levels, induced by altering ventilatory inspiratory and expiratory ratios, lead to non-steady state arterial blood oxygen (P_aO_2) levels. While those studies affirm

that exposure to non-steady state F_iO_2 induces non-steady state P_aO_2 levels, there is an absence of peer-reviewed publications assessing the impact of non-steady state F_iO_2 and P_aO_2 upon functional activity within the human cerebral cortex. Our objective for this study was to address that void.

To inform our understanding of the central nervous system's functional response to non-steady state F_iO_2, we measured prefrontal cortical activity during a cognitive task immediately following exposure to non-steady F_iO_2 and again 120 seconds later following exposure to steady state F_iO_2. This enabled us to test the following hypotheses: 1) Following exposure to non-steady state F_iO_2, P_aO_2 levels will reflect the F_iO_2 at the time which the sample was obtained; 2) The prefrontal cortex will achieve a different level of activation during a cognitive task following exposure to non-steady state F_iO_2 when compared to exposure to steady state F_iO_2; and 3) Exposure to increased F_iO_2 levels, both steady and non-steady state, will be followed by increased levels of systemic proinflammatory serum analytes.

2.0 MATERIALS AND METHODS

The objective of this study was to define the neurophysiologic and systemic responses to non-steady state levels of inspired oxygen concentrations at barometric pressures of 749 mmHg (normobaric pressure at the study site), 565 mmHg (equivalent to an altitude of 2438 meters or 8,000 feet), and 494 mmHg (equivalent to an altitude of 4572 meters or 15,000 feet). Measurements of arterial blood gas levels and prefrontal cortical brain activity were obtained from healthy volunteers during exposure to non-steady state and steady-state F_iO_2.

The study protocol was approved by the Institutional Review Board of University Hospitals, STUDY20191540 and the United States Air Force Human Research Protection Office (HRPO), Protocol Number: FWR20200056X. Candidate study participants were required to be non-smokers between the ages of 18-61 years, and without exposure to a high altitude environment >8,000 ft. within the previous two weeks. Exclusion criteria included a medically conferred diagnosis of pulmonary and/or cardiac disease, a current or previous neurologic issue (e.g. epilepsy or seizure disorder), known history of sickle cell disease or sickle cell trait, elevated risk for bleeding or a bleeding disorder, recent (within the past 5 years) history of inner ear problems, a positive urine pregnancy test or currently attempting pregnancy, or a history of claustrophobia. Upon verifying the absence of exclusion criteria, all candidate participants were provided with, and then signed an informed consent document.

To establish an appropriate sample size, we first conducted a series of preliminary studies in which patterns of prefrontal cortical activity were assessed with functional near infrared spectroscopy during a task-on and task-off cognitive challenge. During that testing, participants were exposed to both non-steady state and steady state F_iO_2 conditions, as described below. Outcomes from those studies revealed that an N=24 would provide sufficient data to achieve a minimum statistical power of 0.80 at a two-tailed significance of < 0.05 to detect differences in prefrontal cortical activity during pegboard testing between exposures to non-steady state and steady state F_iO_2.

A detailed explanation of the experimental protocol and study methods follows (see **Figure 1**).

2.1 Health Screening & Protocol Familiarization. Upon arrival for the day of experimental exposure, participants were queried about current medications followed by measurements of

height and weight, body temperature, vital signs, and self-reported outcome of their most recent coronavirus disease (COVID) test. Those assessments were followed by a focused neurological and physical examination performed by a licensed clinician.

Participants were next instructed on procedures that would occur during the experimental exposures. This included a practice session on the Grooved Pegboard test (Model 32025 Lafayette Instrument, Lafayette IN, USA) which was employed to activate the prefrontal cortex using a task-on/task-off paradigm *(Bakhshipour et al., 2021)* executed in sequence three times. The pegboard contains 25 holes with randomly positioned slots in which metal pegs can be placed. The pegs have a key shape along one side and must be rotated to match the hole before they can be inserted. During the 20-second "task-on" phase, participants were instructed to pick up the pegs, one at a time, and place them into the board. When cued by the researcher for the 20-second "task-off" phase, participants were instructed to stop placing pegs, not move their hands or speak, and try to clear their minds. Participants were coached to not achieve a personal best during any of the tests. Rather, the goal was to complete the task as consistently as possible.

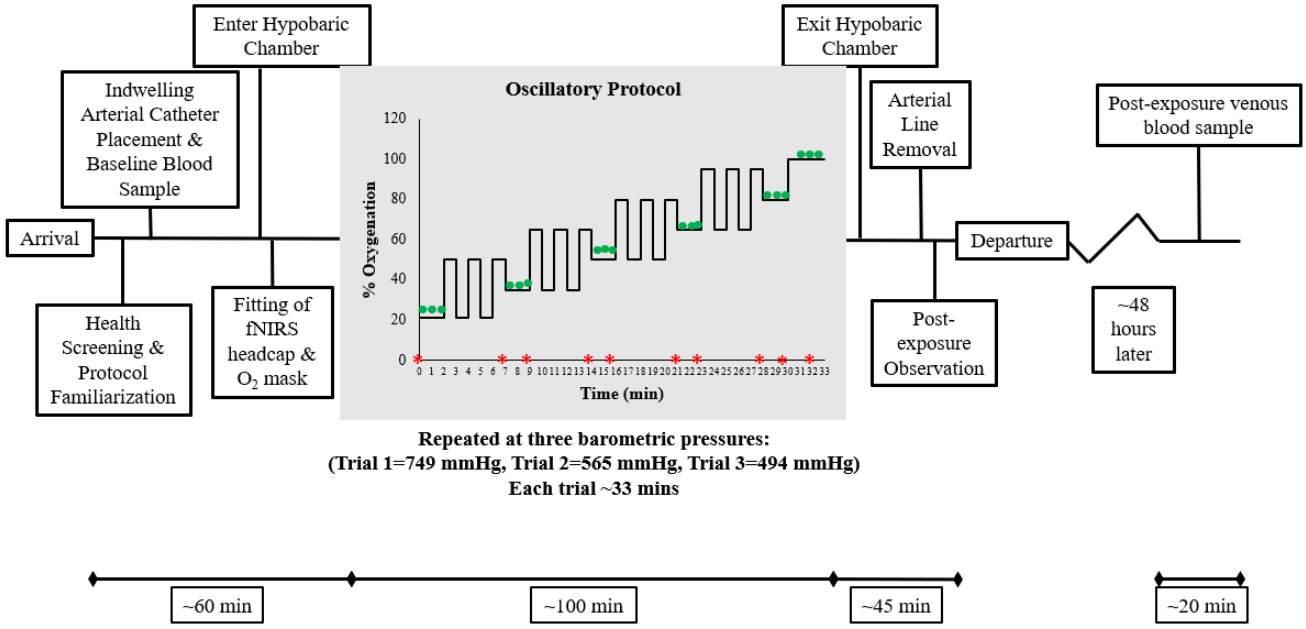

Figure 1. Study data collection overview

This figure illustrates the study protocol at each barometric pressure. The portion of the study in which the participant was exposed to steady-state and non-steady state inspired oxygen is within the gray shaded box. Each exposure to non-steady-state oxygen appears as a series of cyclic square waves. Green circles represent the time points of each pegboard test. Red asterisks represent the time points of each arterial blood sample.

2.2 Indwelling Radial Arterial Catheter Placement. With the study participant seated comfortably, an Allen's test was performed to ensure adequate collateral perfusion throughout both the right and left hands *(Al-Hakim et al., 2019)*. A small heating pad was then placed into

the participant's non-dominant hand to promote vasodilation of the target artery and the wrist was prepped and draped to provide a sterile field. A 1.0 milliliter (mL) subdermal injection of 1% lidocaine was injected into ventral aspect of the wrist to provide local anesthesia. Using ultrasound guidance, a 20 gauge angiocatheter was inserted through the anesthetized area into the radial artery and advanced until a flash of blood was observed in the catheter. The catheter endcap was removed, the catheter's internal stylet withdrawn, and the catheter secured in place with gauze, tape, and a sterile transparent film dressing. One end of a 6-inch extension tubing was attached to the hub of the arterial catheter, with a three-way stopcock attached to the other end. A 500 mL warmed bag of normal saline was placed into a pressure cuff, and the output of the bag attached to the three-way stopcock via a 60-inch intravenous tubing gravity set.

2.2.1. Baseline Blood Sample Collection for Serum Analyte Analyses. Following placement of the arterial catheter, a single 8 mL arterial blood sample was obtained via the three-way stopcock, using a 10 mL syringe. Blood was then injected into an 8.5 mL BD Vacutainer® tiger top serum separator tube (Benton, Dickinson & Company, Franklin Lakes, NJ, USA) and the tube was centrifuged at 3000 revolutions per minute (rpm) for 8-10 minutes. The separated serum was pipetted into 1.5 mL Eppendorf tubes, which were immediately placed into dry ice for transport to -80°Centigrade (C) storage.

2.3 Hypobaric Chamber. Following placement of the indwelling arterial catheter, the study participant entered the human hypobaric chamber (Silvan Industries, Marinette, WI, USA). The chamber was 16 feet (ft) long by 7 ft. wide by 7.5 ft. tall, and able to accommodate 4-6 persons. Although structurally capable of depressurizing to an atmospheric pressure of 8.17 mmHg, equivalent to an altitude of 30,480 meters (m) (100,000 ft), it was programmed to never exceed a barometric pressure below 226 mmHg, which is equivalent to an altitude of 9144 m (30,000 ft).

2.4 Functional Near Infrared Spectroscopy (fNIRS). Once seated inside the chamber, an fNIRS microfiber headcap was placed securely across the participant's scalp and connected to the NIRScout system (NIRx Medical Technologies, LLC, Glen Head, NY, USA). The fNIRS system was used to detect, measure, and quantify changes in the brain's functional response to stimuli by measuring changes in oxygenated and deoxygenated hemoglobin in cortical areas *(Tanaka et al., 2014)*. Based upon the brain's functional response or lack of response to stimuli, neuronal activity within discrete regions can increase, decrease, or remain the same. The subsequent level of activity modifies the volume of blood delivered to those brain regions, leading to a brief change in the concentration of oxygenated and deoxygenated hemoglobin *(LaManna, 2007)*. Patterns of prefrontal cortical brain activation patterns were measured with fNIRS throughout pegboard task-on/task-off sequences.

The fNIRS headcap was equipped with 32 optodes consisting of 16 light emitting diodes (sources) and 16 receivers (detectors). Optode locations concurred with the bilateral prefrontal cortices. A dark cloth hood was then placed over the headcap to minimize ambient light intrusion to the optodes while also reducing risk of optode movement. Signal quality of optodes was confirmed using internal calibration sequences of the system's software (nirsLAB, NIRx Medical Technologies, LLC, Glen Head, NY, USA). If poor signal quality was detected, the hood was removed and the offending optode adjusted. Signal quality was again assessed, and those steps repeated until desired results were attained. One final measurement of signal quality was conducted after placement of the oxygen delivery mask on the participant, as described below.

Continuous fNIRS data collection began at the onset of the study protocol and was recorded throughout the course of the study, which was approximately 120 minutes' duration.

2.4.1. fNIRS Analysis. Acquisition data files were downloaded from the fNIRS system computer and imported into Homer3 open-source software in MATLAB R2022a (The Mathworks, Inc., Natick, Massachusetts, USA) for analysis *(Huppert et al., 2009)*. Preprocessing of data included selecting, from the entire data stream, only those sections occurring within the pegboard "task-on" and corresponding "task-off" periods with 2-seconds of data on either side. This condensed the data file into 128 discrete conditions of 20 seconds duration per condition of task-on or task-off. The condensed dataset was uploaded to the Homer3 GUI where a software pipeline converted raw data to "beta values" for each of the 128, 20-second discrete data conditions. Each data channel was assessed for signal strength and flagged for additional review if the signal strength or the moving average of standard deviations exceeded pre-determined threshold levels. In those cases, we employed recursive principle component analyses as defined by Yücel *(Yücel et al., 2013)*. In addition, each channel was assessed for motion artifact. If the artifact involved multiple channels and exceeded pre-established thresholds, the entire 20-second data condition was rejected and excluded from further analyses. A high-pass and low-pass band filter was applied over the remaining data set. The optical density signals were then converted to oxyhemoglobin and deoxyhemoglobin concentrations followed by block averaging of each of the 128, 20-second data conditions. General Linear Model (GLM) analysis was then used to estimate the hemodynamic response function (HRF) *(Ye et al., 2009)*. Values for both oxyhemoglobin and deoxyhemoglobin were derived and exported to Statistical Analysis Software (SAS) version 9.4 (SAS Institute, Inc., Cary, NC) for further statistical analysis.

Upon completion of signal processing, we then determined patterns of prefrontal cortical brain activity during pegboard testing, first immediately upon cessation of non-steady state F_iO_2, and then following 120 seconds of exposure to steady state F_iO_2. This was accomplished by comparing levels of prefrontal cortical activity during the first 20-second pegboard "task-on" time period with the following 20-second "task-off" time period. We defined the difference between levels of prefrontal cortical activity between those two conditions as "brain activation." We then compared levels of prefrontal cortical activation between pegboard Task #1, which occurred immediately after cessation of non-steady state F_iO_2, with pegboard Task #3 which occurred following 120 seconds of steady state F_iO_2 exposure.

2.5 Delivery of non-steady state FiO2. Following placement of the fNIRS headcap and system calibration, a gel foam-sealed facemask (Hans Rudolph Inc., Shawnee, KS, USA) was strapped securely over the participant's nose and mouth. A 2-way non-rebreather T-shape valve (Hans Rudolph, Series 2700) was inserted into the single large bore opening on the front of the mask. The left side of the connector was attached to an inspiratory circuit while the right side of the connector was attached to the expiratory circuit. A one-way valve within the inspiratory circuit adjacent to the facemask, coupled with constant flow of gas through both the inspiratory and expiratory circuits, insured that the participant did not rebreathe previously exhaled gas.

Delivery of precise oxygen concentrations was achieved by attaching the inspiratory side of the circuit to a PM5200M Air/Oxygen Blender (Precision Medical Inc., Northampton, PA USA). The blender was connected to compressed air (21% oxygen and 79% nitrogen) and oxygen (100%) supply lines and used to titrate specific oxygen concentrations delivered to the study participant. A BIOPAC MP160 data acquisition and analysis system (BIOPAC Systems,

Inc. Goleta, CA) with the BIOPAC oxygen (O_2) 100C Module and a carbon dioxide (CO_2) 100C Module was attached to the participant's face mask to provide a continuous measure of actual mask levels of F_iO_2, CO_2, and respiratory rate. An additional O_2 100C Module was connected to the analyzer to monitor ambient O_2 levels within the hypobaric chamber.

As illustrated in Figure 1, the participant was exposed to steady-state 21% F_iO_2 for three minutes duration. A baseline ABG sample was then obtained from the indwelling arterial catheter using a syringe treated with dry lithium heparin. That initial ABG sample, as well as all subsequent ABG samples, were immediately passed from inside the hypobaric chamber to the outside via a small, sealed steel tube passage. Once received by a research team member outside the hypobaric chamber, the blood sample was immediately injected (within 1-2 minutes) into an iSTAT blood analyzer (Abbott Point of Care, Princeton, NJ, USA) equipped with a CG8+ cartridge for measurement and calculations of ionized sodium, potassium and calcium, Glucose, Hematocrit, Hemoglobin, potential of hydrogen (pH), partial pressure of carbon dioxide ($PaCO_2$), partial pressure of oxygen (P_aO_2), total carbon dioxide content (TCO_2), bicarbonate (HCO_3-), base excess (BE), and oxygen saturation (SaO_2).

2.6 Non-Steady State/Steady State FiO2 Exposures and Arterial Blood Gas Sampling. Following collection of the initial arterial blood sample, the participant executed the pegboard task for 20 seconds, and then rested quietly for 20 seconds before completing two additional pegboard task-on/task-off sequences. Following the third task, the first sequence of non-steady state F_iO_2 exposure was initiated by a rapid increase from 21% to 50%, where it was maintained for 60 seconds, followed by a return to 21% F_iO_2 that was maintained for 60 seconds. That non-steady state cycle was repeated a second and third time. Following the third non-steady state cycle, the F_iO_2 was reduced to 35% (the midpoint between 21% and 50%) and participants completed the three task-on and task-off Grooved Pegboard sequence. Figure 1 illustrates that following the third oscillation of each F_iO_2, a 0.5 mL arterial blood sample was obtained from the arterial catheter line, followed by a 0.5 mL flush of normal saline. The F_iO_2 was then maintained at a *steady state* level for 120 seconds, during which time the participant again completed the three task-on and task-off Grooved Pegboard sequence. At the completion of the pegboard tasks, a second (companion) 0.5 mL arterial blood sample was obtained, followed by a 0.5 mL heparinized saline (100 u/mL) flush to maintain catheter line patency. This pattern of non-steady state F_iO_2 oscillations, arterial blood gas sampling, and pegboard task-on/task-off sequences was repeated at F_iO_2 levels of 50% ± 15%, 65% ± 15%, and 80% ± 15%, as illustrated in Figure 1. Following the final non-steady state F_iO_2 exposure, the F_iO_2 was increased to 100% and maintained for 120 seconds, at which point participants completed a final series of three pegboard task-on/task-off sequences, followed by collection of a single 0.5 mL arterial blood sample.

After completing the initial 33-minute exposure protocol conducted at 749 mmHg (Trial 1), the hypobaric chamber was depressurized to a barometric pressure of 565 mmHg, paralleling an altitude of 8,000 ft. The same protocol of exposure to F_iO_2 oscillations, arterial blood sampling, and pegboard task-on/task-off sequences was again delivered over the next 33-minutes (Trial 2). The hypobaric chamber was then depressurized to a barometric pressure of 494 mmHg, paralleling an altitude of 15,000 ft and same exposure protocol repeated for the third and final time (Trial 3).

Following completion of Trial 3, the chamber was slowly repressurized over a 10-15 minute period. Upon reaching 749 mmHg, the participant was escorted from the chamber, seated

in a chair, and the arterial line removed. The participant was monitored for 30-60 minutes to insure absence of any potential adverse effects resulting from hypobaric conditions or arterial line placement, and then released.

2.7 Post-Exposure Study Visit. Within 48 hours following the experimental exposure, a member of the investigative team met with participant to assess the site of the arterial catheterization and to obtain a post-exposure blood sample for proinflammatory serum analyte analysis. At that time a tourniquet was applied approximately 2-3 inches above the right or left antecubital vein. A 23-gauge butterfly needle with tubing was used to puncture the vein. An 8.5 mL BD Vacutainer® serum separation tube was attached to the butterfly tubing, followed by collection of ~8 mL of venous blood. The venous sample was processed in the same manner as the prior arterial sample, with serum stored at -80°C until analyses.

2.8 Serum Analyte Analyses. Blood serum samples were collected prior to exposure to non-steady state F_iO_2 and hypobaria and again 48 hours after experimental exposure. These serum samples were analyzed using multi-array technology (QuickPlex 120; MesoScale Diagnostics, Rockville, MD) coupled with the V-PLEX neuroinflammation panel (Catalog No. K15210D). To establish measurement reproducibility, each sample was divided between two adjacent wells of each 96-well plate. The neuroinflammation panel included the proinflammatory plate measuring interleukin 1 beta (IL-1β), interleukin 2 (IL-2), interleukin 4 (IL-4), interleukin 6 (IL-6), interleukin 8 (IL-8), interleukin 10 (IL-10), interleukin 13 (IL-13), tumor necrosis factor alpha (TNF-α), and interferon-gamma (IFN-γ). The chemokine plate measured monocyte chemoattractant protein-1 (MCP-1), monocyte chemoattractant protein-4 (MCP-4), eotaxin, macrophage inflammatory protein-1 alpha (MIP-1α), eotaxin-3, thymus activation regulated chemokine (TARC), macrophage inflammatory protein-1 beta (MIP-1β), macrophage-derived chemokine (MDC), and interferon gamma inducible protein-10 (IP-10). The cytokine plate measured interleukin 1 alpha (IL-1α), interleukin 5 (IL-5), interleukin 7 (IL-7), interleukin 12 (IL-12), interleukin 15 (IL-15), interleukin 16 (IL-16), interleukin 17A (IL-17A), tumor necrosis factor beta (TNF-β), and vascular endothelial growth factor A (VEGF-A). The angiogenesis plate measured basic fibroblastic growth factor (bFGF), vascular endothelial growth factor C (VEGF-C), vascular endothelial growth factor D (VEGF-D), vascular endothelial growth factor receptor 1 (Flt-1), placental growth factor (PlGF), and tyrosine kinase 2 (Tie-2). The vascular injury plate measured serum amyloid A (SAA), C-reactive protein (CRP), intercellular adhesion molecule-1 (ICAM-1), and vascular cell adhesion molecule-1 (VCAM-1).

2.9 Statistical Approach. Comparisons of participants' race, age, sex, and body mass index (BMI) were tested using Fisher's Exact test and Wilcoxon Rank Sum test. fNIRS-derived measures of cortical activation levels within each brain region during pegboard Task #1 and pegboard Task #3 were explored using paired *t*-tests or Wilcoxon Signed Rank tests. ABG values obtained following exposures to non-steady state F_iO_2 and again after steady-state F_iO_2 was sustained for 120 seconds were summarized as mean, standard deviation (SD), and range (minimum, maximum) and then compared using paired *t*-tests or Wilcoxon Signed Rank tests. Serum analytes measured at baseline and again at 48 hours following the experimental exposures to hypobaria and to non-steady state and steady-state F_iO_2 were evaluated using the same approach. The false discovery rate (FDR) method was applied to control Type I error from multiple comparison testing. All tests were two-sided and adjusted *p*-values from the FDR less

than 0.05 were considered to be statistically significant. Data were analyzed using SAS version 9.4 (SAS Institute, Inc., Cary, NC) and Statistical Package for Social Sciences (SPSS) version 28 (IBM Corp; Armonk, NY).

3.0 RESULTS

Thirty-seven candidates received a verbal description of the study protocol and provided written informed consent to participate. Of those 37, seven withdrew prior to participating due to scheduling conflicts or concerns regarding COVID. Of the remaining 30 persons who began the study, six were excluded from continuing the protocol following a vasovagal response during arterial catheter placement. The remaining 24 participants completed all phases of the protocol. Their basic demographics are presented in **Table 1**; there were no difference between male and female study participant's age or BMI.

Table 1. Study participant demographics

No age or BMI differences were found between males and females.
[a]p-value from Fisher's Exact test.
[b]p-values from Wilcoxon Rank Sum test.

Sex	**Race**	**Age (years)** M ± SD *(Range)*	**BMI (kg/m^2)** M ± SD *(Range)*
Males n =17	Asian = 2 Black = 5 White = 10	31.12 ± 11.03 *(21-57)*	28.80 ± 5.52 *(22.12-45.84)*
Females n =7	Asian = 2 Black = 0 White = 5	29.57 ± 6.29 *(24-42)*	28.89 ± 5.77 *(21.07-39.30)*
***p*-value**	0.2020[a]	0.8731[b]	0.9241[b]

3.1 Non-Steady State/Steady State FiO2 Exposure. Continuous tracing from the BIOPAC oxygen sensor, attached to the study participant's facemask, validated that the F_iO_2 delivered to the participant matched the intended output from the air/oxygen blender. The signal hysteresis depicted in **Figure 2**, especially at the top of each square wave, represents nitrogen washout from the lungs, which can take several minutes *(Culver, 2012)*. The hysteresis/nitrogen washout reveals the heterogeneity in lung ventilation and confirms that a steady-state, homogenous level of oxygen within the lungs was not achieved during the 60-second cycle time of each F_iO_2 oscillation.

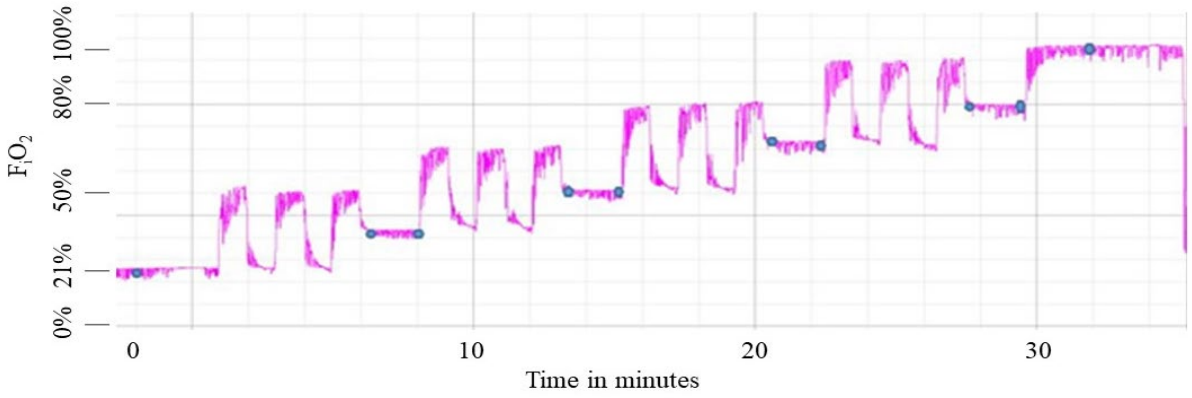

Figure 2. Output from mask oxygen sensor

This graph displays the output from the mask oxygen sensor from one study participant. The x-axis is time in minutes with each block representing two minutes. The y-axis is oxygen concentration measured within the mask, with each block representing 8.0 percent. The blue circles represent the time points of each arterial blood sample. The series of three pegboard tests (not indicated on this figure) were initiated after each collection of each arterial blood sample.

3.2 Arterial Blood Gas Results. Table 2 illustrates that during normobaric ambient pressures (749 mmHg), P_aO_2 levels measured during exposure to steady state 21% F_iO_2 were 95.63 ± 13.21 mmHg (mean ± 1 SD), while exposure to steady state 100% F_iO_2 produced P_aO_2 levels of 541.83 ± 47.62 mmHg. Those values were within the anticipated range for healthy persons *(Crapo et al., 1999)*. Table 2 also presents P_aO_2 levels measured during exposure to steady state 21% and 100% F_iO_2 at the simulated altitudes of 8,000 ft (565 mmHg) and 15,000 ft (494 mmHg). Those P_aO_2 levels were also within anticipated ranges *(Gonzalez-Garcia et al., 2020)*. Accompanying values of P_aCO_2, pH, HCO3, S_aO_2, glucose, and hematocrit are provided in Supplemental Tables 1-6.

Values of P_aO_2 measured at the conclusion of each non-steady state F_iO_2 sequence were significantly greater than P_aO_2 values measured 120 seconds later during exposure to steady state F_iO_2 (Table 2). This pattern was consistent during all non-steady states F_iO_2 sequences administered at 749 mmHg (normobaric conditions), 565 mmHg (8,000 ft), and 494 mmHg (15,000 ft). However, the magnitude of difference between P_aO_2 values observed immediately post non-steady state F_iO_2 with those observed following 120 seconds of steady state F_iO_2, increased as ambient environmental pressure decreased. Whereas the mean percent change was 12.81% during normobaric conditions at 749 mmHg, that mean percent change increased to 15.37% for P_aO_2 values measured at 565 mmHg and 17.55% for P_aO_2 values measured at 494 mmHg.

3.3 fNIRS Results. Table 3 reports comparisons of fNIRS contrasts performed during the Grooved Pegboard task immediately following exposure to oscillatory F_iO_2 with those performed during a Grooved Pegboard task following 120 seconds of exposure to steady-state FiO2. We found exposure to non-steady state cyclic $F_iO_2 > 50\%$ and $< 100\%$ led to reduced prefrontal cortical activation levels immediately following 5 minutes of exposure to oscillatory F_iO_2 at both normobaric pressure and during exposure to a reduced barometric pressure of 494 mmHg. These

results are graphically illustrated in **Figure 3.**

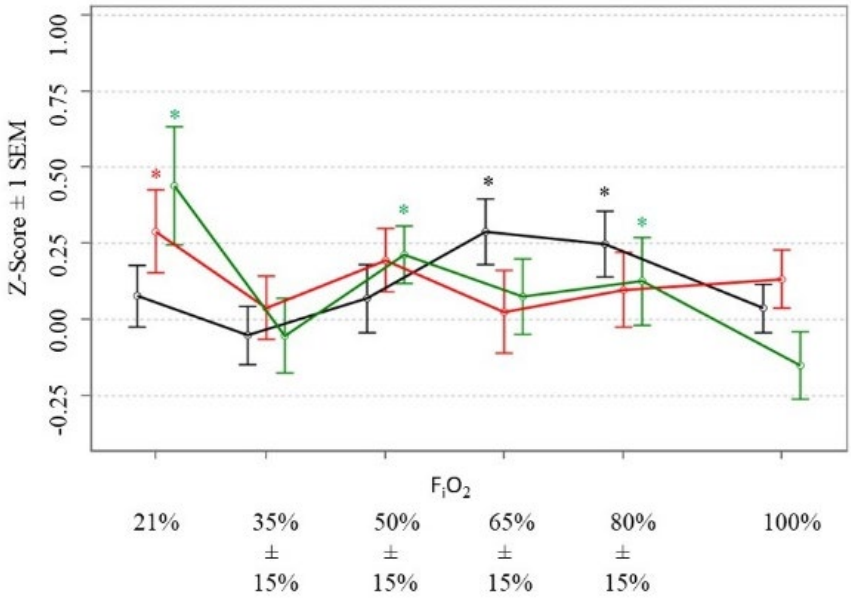

Figure 3. Prefrontal cortical activation

This figure illustrates the z-score ± 1 SEM of prefrontal cortical activation levels as measured by fNIRS between Task #1 and Task #3 at each barometric pressure. The black line represents data generated at 749 mmHg, red is 565 mmHg and green is 494 mmHg. The values for z-scores are staggered on the x-axis only for the purpose of visualization. ***Represents significant differences between Task #1 and Task #3 as reported in Table 3.***

Table 2. Arterial Blood P_aO_2 Comparisons

Comparisons of arterial blood P_aO_2 sampled immediately following 5 minutes of exposure to oscillatory F_iO_2 were compared with those sampled immediately following 120 seconds of exposure to steady-state F_iO_2. Comparisons were performed using paired t-tests unless otherwise indicated.
**p-values from Wilcoxon signed rank test; Adj. p-values from false discovery rate (FDR).*
†Sample size for ABG measurements decreased as a result of one participant whose arterial line catheter became non-functional during the latter part of the experimental protocol.

	F_iO_2 range during non-steady state/steady state hyperoxia exposure	**N†**	**P_aO_2 Measured upon reaching predetermined F_iO_2 level following non-steady state/steady state hyperoxia exposure** (Mean ± SD) *Range*	**P_aO_2 Measured after maintaining predetermined F_iO_2 level for 120 seconds** (Mean ± SD) *Range*	***p*-value**	**Adj. *p*-value**
749 mmHg	21% steady-state	24		95.63 ± 13.21 *(68-122)*	n/a	
(% Change) 17.73%	35% ± 15%	24	216.67 ± 29.53 *(115-264)*	178.25 ± 26.73 *(90-210)*	<.0001	<.0001
13.75%	50% ± 15%	24	296.92 ± 37.53 *(166-356)*	255.50 ± 34.59 *(121-288)*	<.0001	<.0001
9.73%	65% ± 15%	24	382.50 ± 42.99 *(227-431)*	345.29 ± 44.56 *(171-396)*	<.0001	<.0001
10.01%	80% ± 15%	24	470.96 ± 55.59 *(318-548)*	423.83 ± 49.81 *(225-471)*	<.0001*	<.0001
	100% steady-state	24		541.83 ± 47.62 *(385-613)*	n/a	
565 mmHg	21% steady-state	24		66.71 ± 6.10 *(51-83)*	n/a	
21.02%	35% ± 15%	24	154.21 ± 19.72 *(105-195)*	121.79 ± 17.99 *(78-163)*	<.0001	<.0001
18.79%	50% ± 15%	24	218.25 ± 25.10 *(134-264)*	177.25 ± 27.34 *(77-208)*	<.0001	<.0001
11.68%	65% ± 15%	23	274.35 ± 22.37 *(218-301)*	242.30 ± 27.11 *(161-273)*	<.0001	<.0001
9.97%	80% ± 15%	23	336.52 ± 41.60 *(174-391)*	302.96 ± 40.47 *(141-342)*	<.0001	<.0001
	100% steady-state	23		379.29 ± 46.56 *(189-420)*	n/a	
494 mmHg	21% steady-state	23		47.17 ± 5.51 *(36-58)*	n/a	
27.26%	35% ± 15%	23	107.65 ± 16.38 *(77-136)*	78.30 ± 10.61 *(53-93)*	<.0001	<.0001
18.09%	50% ± 15%	23	153.83 ± 20.75 *(93-186)*	126.00 ± 17.22 *(79-152)*	<.0001	<.0001
13.64%	65% ± 15%	23	199.26 ± 25.32 *(111-229)*	172.09 ± 23.19 *(94-197)*	<.0001	<.0001
11.21%	80% ± 15%	23	242.39 ± 21.26 *(184-267)*	215.22± 28.16 *(112-237)*	<.0001	<.0001
	100% steady-state	23		273.22 ± 29.27 *(184-306)*	n/a	

Table 3. Prefrontal Cortical Activation Levels

fNIRS contrasts performed during the Grooved Pegboard task immediately following exposure to oscillatory F_iO_2 were compared with those performed during a Grooved Pegboard task following 120 seconds of exposure to steady-state F_iO_2. Comparisons were performed using paired t-tests unless otherwise indicated.

†Sample size variation is due to artifact rejection which deleted some sequences of fNIRS data.

Table 3						
	F_iO_2 range during non-steady state/steady state hyperoxia exposure	**N†**	**Activation level during pegboard Task #1** (Mean ± SD) *Range*	**Activation level during pegboard Task #3** (Mean ± SD) *Range*	***p*-value**	**Adj. *p*-value**
749 mmHg	21% steady-state	23	0.992 ± 0.918 *(-0.873 - 2.525)*	1.02 ±1.051 *(-1.009 - 2.676)*	0.4625	0.6508
	35% ± 15%	24	0.779 ± 1.029 *(-0.692 - 2.81)*	0.726 ± 0.955 *(-1.153 - 2.576)*	0.5872	0.6508
	50% ± 15%	24	0.662 ± 1.061 *(-0.999 - 2.954)*	0.731 ± 0.822 *(-0.562 - 2.317)*	0.5438	0.6508
	65% ± 15%	24	0.632 ± 0.932 *(-1.36 - 2.692)*	0.92 ± 0.871 *(-0.356 - 2.892)*	0.0146	0.0876
	80% ± 15%	24	0.609 ± 0.815 *(-0.778 - 2.176)*	0.856 ± 0.885 *(-1.071 - 2.649)*	0.0321	0.0963
	100% steady-state	23	0.431 ± 0.969 *(-1.293 - 2.782)*	0.467 ± 0.931 *(-1.243 - 2.988)*	0.6508	0.6508
565 mmHg	21% steady-state	22	0.476 ± 0.987 *(-1.154 - 2.601)*	0.741 ± 1.081 *(-0.723 - 3.614)*	0.0466	0.2190
	35% ± 15%	22	0.756 ± 0.673 *(-0.17 - 2.324)*	0.794 ± 0.845 *(-0.673 - 2.449)*	0.7181	0.8554
	50% ± 15%	24	0.501 ± 1.048 *(-1.548 - 2.951)*	0.695 ± 0.965 *(-1.375 - 2.322)*	0.0730	0.2190
	65% ± 15%	22	0.662 ± 1.056 *(-1.177 - 4.221)*	0.687 ± 0.945 *(-0.819 - 3.677)*	0.8554	0.8554
	80% ± 15%	23	0.555 ± 1.055 *(-1.817 - 2.549)*	0.592 ± 1.031 *(-1.769 - 2.381)*	0.4351	0.6527
	100% steady-state	23	0.791 ± 0.885 *(-1.223 - 2.455)*	0.887 ± 0.916 *(-1.675 - 2.36)*	0.1820	0.3640
494 mmHg	21% steady-state	22	0.434 ± 1.006 *(-1.577 - 2.639)*	0.874 ± 0.764 *(-0.631 - 2.035)*	0.0340	0.0680
	35% ± 15%	23	0.997 ± 1.076 *(-1.041 - 3.164)*	0.943 ± 1.061 *(-0.749 - 3.776)*	0.6663	0.6663
	50% ± 15%	21	0.666 ± 0.791 *(-0.526 - 2.466)*	0.879 ± 1.071 *(-0.674 - 3.611)*	0.0335	0.0680
	65% ± 15%	22	0.798 ± 0.948 *(-0.558 - 2.968)*	0.872 ± 0.949 *(-0.942 - 2.829)*	0.5564	0.6663
	80% ± 15%	22	0.605 ± 0.949 *(-0.715 - 2.583)*	0.726 ± 0.915 *(-0.47 - 3.205)*	0.0271*	0.0680
	100% steady-state	22	0.762 ± 1.075 *(-1.455 - 2.721)*	0.61 ± 0.992 *(-1.361 - 2.439)*	0.1838*	0.2757

**p-values from Wilcoxon signed rank test; Adj. p-values from false discovery rate (FDR).*

749 mmHg (Normobaria). No differences in levels of prefrontal cortical activation occurred at normobaric pressure between Task #1 and Task #3 during exposure to steady state F_iO_2 of 21%. Prefrontal cortical activation levels also did not differ between pegboard Task #1 and Task # 3 during exposure to non-steady state F_iO_2 of 35% ± 15% and F_iO_2 of 50% ± 15%. However, significant differences in prefrontal cortical activation did emerge between Task #1 and Task #3 during exposure to non-steady state F_iO_2 of 65% ± 15% as well as F_iO_2 of 80% ± 15%. At those oxygen concentrations, prefrontal cortical activation levels were significantly lower immediately after exposure to non-steady state F_iO_2 (Task #1) than during steady state F_iO_2 (Task #3). Those differences resolved upon exposure to steady state F_iO_2 of 100%.
565 mmHg (8,000 ft). Prefrontal cortical activation levels only differed between Task #1 and Task #3 at 565 mmHg following exposure to steady state F_iO_2 of 21%. Exposure to increased oxygen concentrations > 21%, presented as either non-steady state or steady state, did not elicit differences in prefrontal cortex activation levels between pegboard Task #1 and Task #3.
494 mmHg (15,000 ft). Prefrontal cortical activation levels at 494 mmHg differed between Task #1 and Task #3 during exposure to steady state F_iO_2 of 21%. Prefrontal cortical activation levels also differed between Task #1 and Task #3 while the participant was exposed to non-steady state F_iO_2 levels of 50% ± 15% and F_iO_2 levels of 80% ± 15%. Those differences resolved upon exposure to steady state F_iO_2 of 100%.
Blood Serum Results. Levels of 37 serum analytes were measured in blood samples obtained at each of the two data collection time points. Of those 37 analytes, serum levels of six analytes differed significantly between values obtained prior to exposure to increased F_iO_2 and hypobaria with those values measured 48 hours after completion of all exposures. Serum levels for those six analytes and outcomes of statistical comparisons are provided in **Table 4**. This table reveals that IL-6, measured by the proinflammatory plate, was increased. The chemokine plate showed increases in IP-10, MCP-1, and MDC. The cytokine plate revealed increased levels of IL-15 while the angiogenesis plate demonstrated that VEGF-D was also increased post-exposure.

Table 4. Serum Analytes

Six serum analyte levels changed significantly from baseline when compared to serum analyte levels measured following exposure to hypobaria and hyperoxia.
*†N=23 due to one missing post-exposure venous blood sample. *p-values from Wilcoxon signed rank test.*
[a]p-values from paired t-tests. Adj. p-values from false discovery rate (FDR).

Analyte	N†	Baseline M ± S.D *(Range)*	Post-Hypobaria & Hyperoxia Exposure M ± S.D *(Range)*	*p*-value[a]	Adj. *p*-value
Proinflammatory Plate (pg/mL)					
IL-6	23	1.367 ± 3.201 *(0.010-15.898)*	1.973 ± 3.790 *(0.305 – 17.981)*	0.014*	0.0268
Chemokine Plate (pg/mL)					
IP-10	23	146.535 ± 76.353 *(34.809 – 394.060)*	245.677 ± 183.548 *(91.328 - 770.989)*	<0.0001*	0.0004
MCP-1	23	84.383 ± 43.204 *(15.264 – 152.951)*	119.536 ± 60.249 *(46.300 - 303.390)*	0.023	0.0268
MDC	23	*495.726 ± 204.249* *(160.135 - 1066.029)*	592.515 ± 207.538 *(324.178 - 1015.837)*	0.004	0.0140
Cytokine (pg/mL)					
IL-15	23	1.464 ± 0.613 *(0.678 – 2.832)*	1.671 ± 0.558 *(0.817 – 2.628)*	0.023	0.0268
Angiogenesis (pg/mL)					
VEGF-D	23	1423.960 ± 343.450 *(853.415 – 2225.042)*	1529.171 ± 417.718 *(824.415 – 2636.861)*	0.023	0.0268

4.0 DISCUSSION

Our objective was to characterize physiologic responses to exposure to both non-steady state and steady state F_iO_2 during normobaric and hypobaric environmental pressures. Primary outcomes included serial measurements of arterial blood gases and prefrontal cortical activity during cognitive challenge. Secondary outcomes included measures of general blood chemistry and quantification of selected serum analytes within the circulatory system both before and after the exposures.

Results indicate that steady state exposure to 21% F_iO_2 during normobaric environmental pressures produced ABG values within anticipated ranges (control condition). Exposure to non-steady state F_iO_2 levels led to transient elevations of P_aO_2 values that were higher upon cessation of non-steady state F_iO_2 than when measured 120 seconds later during steady state exposure to the same F_iO_2 level (Table 2). This pattern of increased P_aO_2 levels following exposure to non-steady state F_iO_2 was consistent across all F_iO_2 ranges, and present at each of the three barometric pressure conditions.

When exposed to both steady state and non-steady state F_iO_2 levels < 50%, prefrontal cortical activation measured during pegboard Task #1 was not different than levels measured 120 seconds later during pegboard Task #3. In contrast, exposure to non-steady state cyclic F_iO_2 > 50% and < 100% led to reduced prefrontal cortical activation levels during Task #1 when compared with levels measured 120 seconds later during Task #3. Those differences emerged at

both normobaric pressure and during exposure to a reduced barometric pressure of 494 mmHg, which simulated an altitude of 15,000 feet.

In addition to acute transient changes within arterial blood gas values and levels of prefrontal cortical activation, we also observed that six serum analyte levels were increased 48 hours following exposure to increased F_iO_2 and hypobaria. Those included IL-6, IP-10, MCP-1, MDC, and IL-15. The vascular endothelial growth factor, VEGF-D, was also increased.

Arterial blood gas values of P_aO_2, measured within two to three breaths following cessation of non-steady state F_iO_2, suggest that the oxygen content within each inspired breath was rapidly conveyed into the circulatory system. During exposure to non-steady state F_iO_2 levels of 65% ± 15% F_iO_2, an atmospheric pressure of 749 mmHg, a P_aCO_2 of 41.9 mmHg with presumed partial pressure of water vapor in the airway of 47 mmHg, and respiratory quotient (R.Q.) of 0.8, the *alveolar* pressure of oxygen (PAO_2) was predicted to be 403.9 mmHg. When accounting for the alveolar-arterial (Aa) gradient, which reduces the partial pressure of oxygen by 5-10 mmHg, the anticipated P_aO_2 within those participants should have been between 389.9-393.9 mmHg. Table 2 reveals that following the non-steady state F_iO_2 sequence of 65% ± 15%, the actual P_aO_2 values were 382.5 ± 42.9 mmHg (mean ± 1 SD), which closely approximates the expected value.

In a recently reported study (*Kelley et al., 2022*), human participants were exposed to 60 second oscillations of 80% F_iO_2 and 20% nitrogen (N_2) and between 70% F_iO_2 and 30% N_2 in a hypobaric chamber at 8000 feet in two exposure cycles of 45 minutes alternating with a 45 minute break. Measurements were taken at ground level before, between, and after the oscillatory exposures and comparisons were made between baseline and hyperoxic oscillatory exposures while remaining at 8000 ft. No differences were found in arterial P_aO_2 across measurement time points but statistically significant reductions in P_aCO_2 were noted between and following the oscillatory exposures. Conversely, our study compared P_aO_2 and P_aCO_2 levels following 120-second exposure of steady-state F_iO_2 of 65% and 80% to P_aO_2 and P_aCO_2 levels obtained following three 60-second oscillations ± 15% of those respective steady-state values at 8000 feet. Key differences between the two experimental designs prevent meaningful comparisons of our study with the Kelley et al. publication. Additional barriers to comparing the two studies include the failure of the prior report to specify the blood gas analyzer used, the lack of explanation for the very low P_aCO_2 levels at baseline and the omission of pH, bicarbonate, and other ABG components that would allow interpretation, and ambiguity whether baseline blood gas measurements used for statistical comparisons were obtained at sea level or at 8000 feet prior to oscillatory exposure.

If significant mixing occurred between newly inspired oxygen content contained within each inspiration with preexisting oxygen content within the residual lung volume, the P_aO_2 value measured following each non-steady state F_iO_2 sequence would have been much higher. During the non-steady state F_iO_2 sequence of 65% ± 15%, the alveolar air equation estimates that an F_iO_2 of 80%, which was the peak F_iO_2 prior to the drop to 65% F_iO_2, would produce P_aO_2 values of 499-504 mmHg *(Rahn, 1949)*. If "mixing" occurred between an existing residual lung volume of gas containing 80% F_iO_2 with an incoming gas containing an F_iO_2 of 65%, the predicted P_aO_2 would have been ~ 440.5 mmHg. However, actual P_aO_2 levels were not in that range; they were instead 382.5 ± 42.9 mmHg. This suggests that during the two to three breaths occurring during the transition from 80% F_iO_2 to 65% F_iO_2, newly inspired oxygen content was immediately transferred from the alveoli into the circulatory system. This would be consistent with observations by Formenti and Farmery *(Formenti and Farmery, 2017)*, who revealed breath-by-

breath oscillations in P_aO_2 do occur, and those oscillations correspond with the inspiratory and expiratory phases of the respiratory cycle. Their studies suggest that the actual oxygen content within each inspired breath is rapidly transferred across the alveolar epithelium and into the systemic circulation.

Exposure to non-steady state F_iO_2 sequences evoked a systematic and reproducible outcome on P_aO_2 levels, regardless of ambient environmental pressures. In contrast, non-steady state F_iO_2 influences upon prefrontal cortical activation were less systematic and were constrained to F_iO_2 exposures > 50% but < 100%. Potential mechanisms influencing those changes in prefrontal cortical activation levels have been informed by studies characterizing the impact of increased F_iO_2 on cerebral perfusion. Those studies *(Damato et al., 2020;Damato et al., 2022)*, conducted under normobaric conditions, revealed that cerebral perfusion is unaffected by F_iO_2 levels ≥ 21% but ≤ 50%. Beginning with F_iO_2 levels of 60%, cerebral perfusion begins to decline and continues to fall with each incremental increase in F_iO_2. Upon reaching an F_iO_2 of 80%, cerebral perfusion is reduced by ~ 25% of baseline values (mean ± 1 SD), dropping from 46.16 ± 10.11 milliliters per minute per 100 grams of tissue (mL/min/100g) to 34.58 ± 8.59 mL/min/100g. During exposure to 100% F_iO_2, cerebral perfusion is 32.46 ± 7.24 mL/min/100g, a five percent reduction from levels observed during exposure to 80% F_iO_2. Collectively, these findings suggest that exposure to F_iO_2 levels of ~ 60% evokes onset of neurovascular constriction. Increasing F_iO_2 beyond 60% prompts further neurovascular constriction, which becomes maximal during exposure to F_iO_2 levels between 80% -100%.

Our collective observations from this and prior studies suggest that 1) P_aO_2 levels are increased following exposure to non-steady state F_iO_2 compared to when measured following the subsequent 120 seconds of steady state F_iO_2 (Table 2), and 2) F_iO_2 levels ≥ 60% reduce cerebral perfusion via *neurovascular constriction (Damato et al., 2022)*, and finally, 3) lowering the F_iO_2 from 100% to 21% leads to *neurovascular dilation* with restoration of cerebral perfusion to baseline levels *(Damato et al., 2022)*. Those findings lead us to suspect that exposure to non-steady state, cyclic F_iO_2 levels within the range of 65% ± 15% induces non-steady state, cyclic neurovascular constriction and dilation. During exposure to 80% F_iO_2, the peak level delivered during the non-steady state F_iO_2 sequence of 65% ± 15%, maximal neurovascular constriction with a concomitant reduction in cerebral perfusion would have existed. We believe the reduced levels of prefrontal cortical activity observed during pegboard Task #1 reflected the reduced cerebral perfusion occurring at the peak F_iO_2 during non-steady state exposures.

Due to the inherent circulatory delay between the lungs and brain *(Oldendorf and Kitano, 1967; Mapleson, 1973)*, the change in F_iO_2 from 80% to 65% followed by neurovascular dilation with increased cerebral perfusion, would not have occurred until after completion of pegboard Task #1. Beginning with pegboard Task #3, which commenced following 120 seconds of steady state F_iO_2, neurovascular dilation with increased cerebral perfusion would have achieved a constant level. The relative increase of cerebral perfusion at F_iO_2 of 65% versus that following exposure to an F_iO_2 of 80% would have led to increased oxygen delivery. We believe that during pegboard Task #3, the increase in cerebral perfusion and oxygen delivery could have accounted for the increased prefrontal cortical activation levels that we observed. While that hypothesis is biologically plausible, confirming or refuting it would have required additional studies and experimental techniques on cortical connectivity that were beyond the intent and scope of this study.

In addition to the changes in P_aO_2 and levels of prefrontal cortical activation that emerged during exposure to non-steady state F_iO_2, we also observed increased levels of six blood serum

analytes 48 hours later following conclusion of the experimental protocol. Comparison of our serum analyte levels to previously published reports is limited by different analysis techniques (enzyme-linked immunosorbent assay (ELISA)) vs. the more sensitive multi-array technology we used) and the scarcity of studies documenting inter-subject variation and temporal changes in baseline levels within non-clinical populations. Two studies conducted in healthy individuals concluded that significant variability exists in baseline levels between healthy individuals, and most cytokines remain stable across serial measurements (Biancotto et al., 2013; Wu et al., 2017). The baseline and post-exposure serum analyte levels we report appear to reside within published normative reference ranges (Biancotto et al., 2013; Glasgow et al., 2009; Lev et al., 2021; Mielnik et al., 2012; Purzycka et al., 2022). However, comparisons are limited between ELISA-derived values and those obtained from ultrasensitive assay methods that are essential for characterizing cytokine levels (Wu et al., 2017). More importantly, the increase in serum analytes levels in our study concurs with prior observations that exposure either to steady state or non-steady state F_iO_2 levels ≥ 50% elicits onset of proinflammatory biochemical cascades within the pulmonary epithelium and other cell types *(Boehme et al., 2019)*. In addition, placement of the radial artery catheter could also have initiated release of several of the proinflammatory serum analytes presented in Table 4. Although baseline levels of MCP-1 have been reported to vary across time in healthy individuals (Biancotto et al., 2013), MCP-1 influences movement of monocytes out of the bloodstream, across the endothelium and into the tissues to engage in immunologic surveillance and inflammatory responses *(Deshmane et al., 2009)* and could explain the increase we observed. Determining the specific mechanisms underlying increased analyte levels is beyond the scope of this project but may represent an adaptive or maladaptive physiological stress response.

4.1 Strengths and Limitations. The intent of this study was to characterize the physiologic responses of healthy individuals to exposure of both steady state and non-steady F_iO_2 levels above 21%. Specific F_iO_2 levels were delivered in a non-steady state, square wave cycle which ranged ± 15% around a pre-specified level or "dose" of oxygen. That experimental design was intended to model oxygen delivery provided by aviation life support systems that employ onboard oxygen generating systems, some of which can potentially deliver oxygen concentrations of ± 15% around a pre-defined level. Study participants were exposed to those non-steady F_iO_2 levels within a hypobaric chamber that provided three different barometric pressures: 749 mmHg, which was the normobaric pressure of the study location, 565 mmHg paralleling an altitude of 8,000 feet, and 494 mmHg, which was equivalent to an altitude of 15,000 feet. Each pressure was chosen as representative of cockpit pressures encountered by tactical aviators. Simultaneous and conscious manipulation of the key experimental variables of F_iO_2 and environmental pressure could induce inherent confounds to data analyses and interpretation, and thereby, present a study weakness. In contrast, our *a-priori* intent was to recreate an exposure matrix of non-steady state F_iO_2 levels delivered within a normobaric and hypobaric environment, thereby emulating the life support system and ambient cockpit pressures that many tactical aviators routinely experience.

Statistical analyses revealed that P_aO_2 levels differed immediately following exposure to non-steady state F_iO_2 compared to P_aO_2 levels 120 seconds later during steady state exposure to steady-state F_iO_2. Levels of prefrontal cortical activity, which were measured that the same time that the arterial blood gas samples occurred, also differed but only during F_iO_2 exposures ≥ 60%. In addition, six of 37 blood serum analytes differed between baseline and the study endpoint.

However, our experimental design, which included placement of an arterial line catheter, precludes a defensible discussion of how hyperoxia/hypobaria may have contributed to the changes in serum analytes that we observed.

It remains unclear why non-steady state F_iO_2 levels > 50% but < 100% led to changes in prefrontal cortical activation between Task #1 and Task #3 only at normobaric pressure (749 mmHg) and again at a barometric pressure of 494 mmHg, equivalent to 15,000 feet. Figure 3 suggests that at an atmospheric pressure of 565 mmHg simulating an altitude of 8,000 feet, the pegboard Task #1 to Task #3 patterns of prefrontal cortical activation were similar to those seen during at an atmospheric pressure of 494 mmHg, equivalent to 15,000 feet. The difference was that the individual range of prefrontal cortical activation levels at 565 mmHg between pegboard Task #1 to Task #3 was much greater than that observed at either 749 mmHg or 494 mmHg (Table 3). As the participants in our study had never before been inside a hypobaric chamber, their novel experience with depressurization may have led to a temporary state of heightened arousal that subsequently masked statistically changes in prefrontal cortical activation between pegboard Task #1 and Task #3. Acclimatization to the experience of hypobaria at 565 mmHg could have reduced likelihood of anxiety during the transition to the lower barometric pressure to 494 mmHg, enabling changes in changes in prefrontal cortical activation between pegboard Task #1 and Task #3 to be observed during that phase of the study. However, this is only speculation, and no defensible reason exists to exclude those persons who experienced the wider range of variability of prefrontal cortical activation during pegboard testing at 565 mmHg. While a sham condition may have reduced any confounding effect of participant anxiety, the invasiveness of arterial line placement and continued data collection during the decreasing but ever-present exposure risks of the pandemic, precluded this option.

To inform our decision of whether Type I error corrections could be avoided, we identified recent studies of a similar sample size, N=20 *(Kerstein et al., 2017)* and larger N=51*(Wunderlich et al., 2017)* using similar technologies employed in this study. Neither study applied Bonferroni corrections. Nonetheless, we felt that controlling for Type I error could enhance the rigor of our analyses and defensibility of findings. As application of Bonferroni corrections in a study such as this could obscure pertinent findings *(Armstrong, 2014)*, we chose to present all significant findings and annotate those that remained significant following FDR correction. We consider this level of transparency to be a strength rather than a limitation of this study.

We do not believe that this study's limitations impact the significance of our findings that exposure to non-steady F_iO_2 levels are followed by changes in arterial blood oxygen content, changes in prefrontal cortical activation levels, and enhanced systemic levels of proinflammatory serum analytes. Although neurovascular tone was not directly measured in this study, our findings pose the hypothesis that neurovascular constriction and dilation may potentially exist during exposure to non-steady state F_iO_2 levels $\geq$ 60%. If it does indeed occur, executive functioning, cognitive performance, and visuomotor speed and accuracy could be impacted. Addressing that relevant question will require additional studies employing experimental protocols, cognitive assessments, and other physiologic measurement techniques beyond those employed in this study.

5.0 REFERENCES

Al-Hakim, R., Hedge, J.C., Jahangiri, Y., Kaufman, J.A., Galuppo, R., and Farsad, K. (2019). Palmar warming for radial artery vasodilation to facilitate transradial access: A randomized controlled trial. *J Vasc Interv Radiol* 30**,** 421-424.

Armstrong, R.A. (2014). When to use the Bonferroni correction. *Ophthalmic Physiol Opt* 34**,** 502-508.

Asfar, P., Singer, M., and Radermacher, P. (2015). Understanding the benefits and harms of oxygen therapy. *Intensive Care Med* 41**,** 1118-1121.

Bakhshipour, E., Koiler, R., Milla, K., and Getchell, N. (Year). "Understanding the Cognitive Demands of the Purdue Pegboard Test: An fNIRS Study", in: *Advances in Neuroergonomics and Cognitive Engineering*, eds. H. Ayaz & U. Asgher: Springer International Publishing, 55-61.

Bhat, A.A., Mang, H., Rajkumar, S., Kotresh, T., and Singh, U. (2017). On-board oxygen generation using high performance molecular sieve. *Def Life Sci J* 2**,** 380-384.

Biancotto, A.,Wank, A., Perl, S., Cook, W., Olnes, M. J., Dagur, P. K., et al. (2013). Baseline levels and temporal stability of 27 multiplexed serum cytokine concentrations in healthy subjects. *PLoS ONE* 8, e76091.

Boehme, S., Hartmann, E.K., Tripp, T., Thal, S.C., David, M., Abraham, D., Baumgardner, J.E., Markstaller, K., and Klein, K.U. (2019). PO2 oscillations induce lung injury and inflammation. *Crit Care* 23**,** 102.

Brugniaux, J.V., Coombs, G.B., Barak, O.F., Dujic, Z., Sekhon, M.S., and Ainslie, P.N. (2018). Highs and lows of hyperoxia: Physiological, performance, and clinical aspects. *Am J Physiol Regul Integr Comp Physiol* 315**,** R1-R27.

Ciarlone, G.E., Hinojo, C.M., Stavitzski, N.M., and Dean, J.B. (2019). CNS function and dysfunction during exposure to hyperbaric oxygen in operational and clinical settings. *Redox Biol* 27**,** 101159.

Crapo, R.O., Jensen, R.L., Hegewald, M., and Tashkin, D.P. (1999). Arterial blood gas reference values for sea level and an altitude of 1,400 meters. *Am J Respir Crit Care Med* 160**,** 1525-1531.

Culver, B.H. (2012). "Chapter 9 - Pulmonary Function Testing," in *Clinical Respiratory Medicine (Fourth Edition),* eds. S.G. Spiro, G.A. Silvestri & A. Agustí. (Philadelphia: W.B. Saunders), 133-142.

Damato, E.G., Fillioe, S.J., Vannix, I.S., Norton, L.K., Margevicius, S.P., Beebe, J.L., and Decker, M.J. (2022). Characterizing the dose response of hyperoxia with brain perfusion. *Aerosp Med Hum Perform* 93**,** 493-498.

Damato, E.G., Flak, T.A., Mayes, R.S., Strohl, K.P., Ziganti, A.M., Abdollahifar, A., Flask, C.A., Lamanna, J.C., and Decker, M.J. (2020). Neurovascular and cortical responses to hyperoxia: Enhanced cognition and electroencephalographic activity despite reduced perfusion. *J Physiol* 598**,** 3941-3956.

Deshmane, S.L., Kremlev, S., Amini, S., and Sawaya, B.E. (2009). Monocyte chemoattractant protein-1 (MCP-1): An overview. *J Interferon Cytokine Res* 29**,** 313-326.

Dussault, C., Gontier, E., Verret, C., Soret, M., Boussuges, A., Hedenstierna, G., and Montmerle-Borgdorff, S. (2016). Hyperoxia and hypergravity are independent risk factors of atelectasis in healthy sitting humans: a pulmonary ultrasound and SPECT/CT study. *J Appl Physiol (1985)* 121**,** 66-77.

Elliott, L.C.J.J., and Schmitt, M.D.R. (2019). Unexplained physiological episodes: A pilot's perspective. *Air & Space Power Journal* 33**,** 15-32.

Floyd, T.F., Clark, J.M., Gelfand, R., Detre, J.A., Ratcliffe, S., Guvakov, D., Lambertsen, C.J., and Eckenhoff, R.G. (2003). Independent cerebral vasoconstrictive effects of hyperoxia and accompanying arterial hypocapnia at 1 ATA. *J Appl Physiol (1985)* 95**,** 2453-2461.

Formenti, F., Bommakanti, N., Chen, R., Cronin, J.N., Mcpeak, H., Holopherne-Doran, D., Hedenstierna, G., Hahn, C.E.W., Larsson, A., and Farmery, A.D. (2017). Respiratory oscillations in alveolar oxygen tension measured in arterial blood. *Sci Rep* 7**,** 7499.

Formenti, F., and Farmery, A.D. (2017). Intravascular oxygen sensors with novel applications for bedside respiratory monitoring. *Anesth* 72 Suppl 1**,** 95-104.

Glasgow, C.G., Avila, N.A., Lin, J.P., Stylianou, M.P. and Moss, J. (2009). Serum vascular endothelial growth factor-D levels in patients with lymphangioleiomyomatosis reflect lymphatic involvement. *Chest 135*, 1293-1300.

Gonzalez-Garcia, M., Maldonado, D., Barrero, M., Casas, A., Perez-Padilla, R., and Torres-Duque, C.A. (2020). Arterial blood gases and ventilation at rest by age and sex in an adult Andean population resident at high altitude. *Eur J Appl Physiol* 120**,** 2729-2736.

Grayson-Smith, H., and Findlay, J.C. (1946). Liquid oxygen in aircraft. *Chem Rev* 39**,** 397-402.

Griffiths, E.A. (1922). The production of liquid oxygen for use on aircraft. *Transactions of the Faraday Society* 18**,** 224-239.

Huppert, T.J., Diamond, S.G., Franceschini, M.A., and Boas, D.A. (2009). HomER: a review of time-series analysis methods for near-infrared spectroscopy of the brain. *Appl Opt* 48**,** D280-298.

Kelley, E.F., Carlson, A.R., Wentz, R.J., Ziegler, B.L., Johnson, B.D. (2022). Influence of rapidly oscillating inspired O_2 and N_2 concentrations on pulmonary vascular function and lung fluid balance in healthy adults. *Front. Physiol. 13*:1018057.

Kerstein, A., Schüler, S., Cabral-Marques, O., Fazio, J., Häsler, R., Müller, A., Pitann, S., Moosig, F., Klapa, S., and Haas, C. (2017). Environmental factor and inflammation-driven alteration of the total peripheral T-cell compartment in granulomatosis with polyangiitis. *J Autoimmun* 78**,** 79-91.

Lamanna, J.C. (2007). In situ measurements of brain tissue hemoglobin saturation and blood volume by reflectance spectrophotometry in the visible spectrum. *J Biomed Opt* 12**,** 062103.

Lambertsen, C.J., Dough, R.H., Cooper, D.Y., Emmel, G.L., Loeschcke, H.H., and Schmidt, C.F. (1953). Oxygen toxicity: Effects in man of oxygen inhalation at 1 and 3.5 atmospheres upon blood gas transport, cerebral circulation and cerebral metabolism. *J Appl Physiol* 5**,** 471-486.

Lev, S., Gottesman, T., Sahaf Levin, G., Lederfein, D., Berkov, E., Diker, D., et al. (2021). Observational cohort study of IP-10's potential as a biomarker to aid in inflammation regulation within a clinical decision support protocol for patients with severe COVID-19. *PLoS ONE 16*(1), e0245296.

Lodato, R.F. (1989). Decreased O2 consumption and cardiac output during normobaric hyperoxia in conscious dogs. *J Appl Physiol (1985)* 67**,** 1551-1559.

Manatt, S.A. (1981). Onboard oxygen generation systems. *Aviat Space Environ Med* 52**,** 645-653.

Mapleson, W.W. (1973). Circulation-time models of the uptake of inhaled anaesthetics and data for quantifying them. *Br J Anaesth* 45**,** 319-334.

Mattos, J.D., Campos, M.O., Rocha, M.P., Mansur, D.E., Rocha, H.N.M., Garcia, V.P., Rocha, N.G., Silveira Alvares, T., Secher, N.H., Claudio Lucas Da Nobrega, A., and Fernandes, I.A. (2019). Differential vasomotor responses to isocapnic hyperoxia: Cerebral vs. peripheral circulation. *Am J Physiol Regul Integr Comp Physiol*.

Mielnik, P., Chwalinska-Sadowska, H., Wiesik-Szewczyk, E., Maslinski, W, and Olesinska, M. (2012). Serum concentration of interleukin 15, interleukin 2 receptor and TNF receptor in patients with polymyositis and dermatomyositis: Correlation to disease activity. *Rheumatol Int, 32*, 639-643.

Oldendorf, W.H., and Kitano, M. (1967). Radioisotope measurement of brain blood turnover time as a clinical index of brain circulation. *J Nucl Med* 8**,** 570-587.

Purzycka-Bohdan, D., Nedoszytko, B., Zablotna, M., Glen, J., Szczerkowska-Dobosz, A., Nowicki, R.J. (2022). Chemokine profile in psoriasis patients in correlation with disease severity and pruritus. *Int J Mol Sci 23*, 13330.

Rahn, H. (1949). A concept of mean alveolar air and the ventilation-blood flow relationships during pulmonary gas exchange. *Am J Physiol* 158**,** 21-30.

Tanaka, H., Katura, T., and Sato, H. (2014). Task-related oxygenation and cerebral blood volume changes estimated from NIRS signals in motor and cognitive tasks. *Neuroimage* 94**,** 107-119.

Tiboldi, A., Hunyadi-Gulyas, E., Wohlrab, P., Schmid, J.A., Markstaller, K., Klein, K.U., and Tretter, V. (2022). Effects of hyperoxia and hyperoxic oscillations on the proteome of murine lung microvascular endothelium. *Antioxidants (Basel)* 11.

Wohlrab, P., Johann Danhofer, M., Schaubmayr, W., Tiboldi, A., Krenn, K., Markstaller, K., Ullrich, R., Ulrich Klein, K., and Tretter, V. (2021). Oxygen conditions oscillating between hypoxia and hyperoxia induce different effects in the pulmonary endothelium compared to constant oxygen conditions. *Physiol Rep* 9**,** e14590.

Wu, D., Dinh, T. L., Bausk, B. P., and Walt, D. R. (2017). Long-term measurements of human inflammatory cytokines reveal complex baseline variations between individuals. *Am. J. Pathol. 187*, 2620–2626.

Wunderlich, T., Frey, N., Kähler, W., Lutz, M., Radermacher, P., Klapa, S., Koch, I., Tillmans, F., Witte, J., and Koch, A. (2017). Influence of hyperoxia on diastolic myocardial and arterial endothelial function. *Undersea Hyperb Med* 44**,** 521-533.

Ye, J.C., Tak, S., Jang, K.E., Jung, J., and Jang, J. (2009). NIRS-SPM: Statistical parametric mapping for near-infrared spectroscopy. *Neuroimage* 44**,** 428-447.

Yücel, M.A., Selb, J., Cooper, R.J., and Boas, D.A. (2013). Targeted principle component analysis: A new motion artifact correction approach for near-infrared spectroscopy. *J Innov Opt Health Sci* 07**,** 1350066.

Supplemental Table 1: Arterial Blood P_aCO_2 Comparisons. Supplemental Table 1 presents arterial blood sample P_aCO_2 values measured immediately upon reaching the predetermined F_iO_2 level (following the final non-steady-state exposure) with those measured 120 seconds later during steady-state F_iO_2. No significant differences were found. Comparisons were performed using paired *t*-tests unless otherwise indicated. †Sample size decreased as a result of one participant whose arterial line catheter became non-functional during the latter part of the experimental protocol.
*p-value from Wilcoxon Signed Rank test. Adj. p-values from false discovery rate (FDR).

	F_iO_2 range during non-steady state/steady state hyperoxia exposure	**N†**	**P_aCO_2 Measured upon reaching predetermined F_iO_2 level following non-steady state/steady state hyperoxia exposure** (Mean ± SD) *Range*	**P_aCO_2 Measured after maintaining predetermined F_iO_2 level for 120 seconds** (Mean ± SD) *Range*	***p*-value**	**Adj. *p*-value**
749 mmHg	21% steady-state	24		38.87 ± 3.40 *(30.80-44.30)*	n/a	
	35% ± 15%	24	41.13 ± 4.74 *(30.60-49.20)*	40.48 ±4.46 *(29.60-46.70)*	0.1898	0.5694
	50% ± 15%	24	41.79 ± 4.52 *(30.60-48.70)*	41.64 ±4.55 *(28.60-51.90)*	0.7091	0.9591
	65% ± 15%	24	41.81 ± 4.21 *(30.40-48.40)*	42.53 ± 3.91 *(32.10-50.00)*	0.1235	0.5694
	80% ± 15%	24	43.56 ±3.28 *(36.90-48.10)*	42.83 ± 3.70 *(32.90-50.10)*	0.1790	0.5694
	100% steady-state	24		44.02 ± 4.43 *(34.80-50.80)*	n/a	
565 mmHg	21% steady-state	24		34.97 ± 3.91 *(25.40-42.40)*	n/a	
	35% ± 15%	24	39.80 ± 4.41 *(25.80-46.70)*	39.83 ± 4.53 *(24.30-46.90)*	0.9649	0.9649
	50% ± 15%	24	39.68 ± 4.38 *(26.80-45.20)*	40.57 ± 4.66 *(27.10-49.60)*	0.1151	0.5694
	65% ± 15%	23	41.38 ± 3.93 *(31.10-48.20)*	41.80 ± 5.04 *(28.10-56.30)*	0.5261	0.9591
	80% ± 15%	23	42.00 ± 4.62 *(28.90-49.00)*	42.08 ± 4.24 *(30.00-48.00)*	0.8475	0.9591
	100% steady-state	23		42.96 ± 4.17 *(33.40-50.00)*	n/a	
494 mmHg	21% steady-state	23		33.15 ± 2.97 *(29.20-38.50)*	n/a	
	35% ± 15%	23	38.10 ± 5.01 *(28.90-46.90)*	37.89 ± 4.30 *(29.00-44.80)*	0.7007	0.9591
	50% ± 15%	23	39.25 ± 4.48 *(31.10-47.80)*	39.33± 4.52 *(28.70-47.20)*	0.8792	0.9591
	65% ± 15%	23	39.90 ± 4.79 *(27.20-45.50)*	40.02 ± 5.36 *(25.30-48.20)*	0.8418	0.9591
	80% ± 15%	23	39.90 ± 5.36 *(24.00-49.30)*	40.18 ± 5.23 *(26.30-47.60)*	0.6383	0.9591
	100% steady-state	23		41.01 ± 4.89 *(26.10-49.00)*	n/a	

Supplemental Table 2: Arterial Blood pH Comparisons. Supplemental Table 2 presents arterial blood sample pH values measured immediately upon reaching the predetermined F_iO_2 level (following the final non-steady-state exposure) with those measured 120 seconds later during steady-state F_iO_2. Comparisons were performed using paired *t*-tests unless otherwise indicated.
†Sample size decreased as a result of one participant whose arterial line catheter became non-functional during the latter part of the experimental protocol.
*p-value from Wilcoxon Signed Rank test; Adj. p-values from false discovery rate (FDR).

	F_iO_2 range during non-steady state/steady state hyperoxia exposure	**N†**	**pH Measured upon reaching predetermined F_iO_2 level following non-steady state/steady state hyperoxia exposure** (Mean ± SD) *Range*	**pH Measured after maintaining predetermined F_iO_2 level for 120 seconds** (Mean ± SD) *Range*	***p*-value**	**Adj. *p*-value**
749 mmHg	21% steady-state	24		7.40 ± 0.02 *(7.36-7.45)*	n/a	
	35% ± 15%	24	7.40 ± 0.03 *(7.36-7.46)*	7.40 ± 0.03 *(7.35-7.50)*	0.2069	0.6207
	50% ± 15%	24	7.40 ± 0.03 *(7.36-7.47)*	7.40 ± 0.03 *(7.34-7.50)*	0.3845	0.9048
	65% ± 15%	24	7.41 ± 0.03 *(7.35-7.47)*	7.41 ± 0.03 *(7.36-7.48)*	0.9817	0.9817
	80% ± 15%	24	7.40 ± 0.02 *(7.37-7.44)*	7.41 ± 0.03 *(7.36-7.49)*	0.0264*	0.1584
	100% steady-state	24		7.41 ± 0.03 *(7.36-7.47)*	n/a	
565 mmHg	21% steady-state	24		7.43 ± 0.03 *(7.39-7.52)*	n/a	
	35% ± 15%	24	7.40 ± 0.03 *(7.35-7.50)*	7.40 ± 0.03 *(7.37-7.54)*	0.0247*	0.1584
	50% ± 15%	24	7.41 ± 0.04 *(7.35-7.50)*	7.40 ± 0.03 *(7.35-7.49)*	0.0798	0.3192
	65% ± 15%	23	7.40 ± 0.02 *(7.36-7.46)*	7.40 ± 0.03 *(7.37-7.49)*	0.7338	0.9114
	80% ± 15%	23	7.40 ± 0.03 *(7.36-7.48)*	7.40 ± 0.03 *(7.37-7.47)*	0.5769	0.9114
	100% steady-state	23		7.40 ± 0.03 *(7.36-7.45)*	n/a	
494 mmHg	21% steady-state	23		7.45 ± 0.02 *(7.41-7.48)*	n/a	
	35% ± 15%	23	7.41 ± 0.03 *(7.36-7.48)*	7.41 ± 0.03 *(7.37-7.46)*	0.7511	0.9114
	50% ± 15%	23	7.40 ± 0.03 *(7.35-7.47)*	7.40 ± 0.03 *(7.36-7.51)*	0.7595	0.9114
	65% ± 15%	23	7.40 ± 0.04 *(7.35-7.51)*	7.40 ± 0.04 *(7.36-7.55)*	0.9494	0.9817
	80% ± 15%	23	7.41 ± 0.05 *(7.36-7.57)*	7.41 ± 0.04 *(7.36-7.55)*	0.4524	0.9048
	100% steady-state	23		7.41 ± 0.04 *(7.36-7.55)*	n/a	

Supplemental Table 3: Arterial Blood HCO_3 Comparisons. Supplemental Table 3 presents arterial blood sample HCO_3 values measured immediately upon reaching the predetermined F_iO_2 level (following the final non-steady-state exposure) with those measured 120 seconds later during steady-state F_iO_2. Comparisons were performed using paired *t*-tests unless otherwise indicated.
†Sample size decreased as a result of one participant whose arterial line catheter became non-functional during the latter part of the experimental protocol.
*p-value from Wilcoxon Signed Rank test; Adj. p-values from false discovery rate (FDR).

	F_iO_2 range during non-steady state/steady state hyperoxia exposure	**N†**	**HCO_3 Measured upon reaching predetermined F_iO_2 level following non-steady state/steady state hyperoxia exposure** (Mean ± SD) *Range*	**HCO_3 Measured after maintaining predetermined F_iO_2 level for 120 seconds** (Mean ± SD) *Range*	***p*-value**	**Adj. *p*-value**
749 mmHg	21% steady-state	24		24.15 ± 1.65 *(20.50-27.00)*	n/a	
	35% ± 15%	24	25.27 ± 1.94 *(21.10-27.70)*	25.16 ± 1.70 *(20.60-27.50)*	0.5871	0.8614
	50% ± 15%	24	25.82 ± 1.81 *(21.40-29.20)*	25.92 ± 1.75 *(22.30-29.00)*	0.6235	0.8614
	65% ± 15%	24	26.19 ± 1.58 *(22.30-28.60)*	26.63 ± 1.45 *(23.80-29.70)*	0.0310*	0.1860
	80% ± 15%	24	27.11 ± 1.46 *(23.80-29.80)*	27.04 ± 1.42 *(24.60-29.80)*	0.7315	0.8614
	100% steady-state	24		27.67 ± 1.78 *(24.50-31.50)*	n/a	
565 mmHg	21% steady-state	24		23.28 ± 1.49 *(20.50-25.90)*	n/a	
	35% ± 15%	24	24.41 ± 1.52 *(20.00-27.80)*	24.85 ± 1.72 *(20.60-28.40)*	0.0284*	0.1860
	50% ± 15%	24	24.98 ± 1.64 *(20.91-27.40)*	25.05 ± 1.69 *(20.80-28.20)*	0.6969	0.8614
	65% ± 15%	23	25.77 ± 1.73 *(22.10-29.00)*	25.91 ± 2.12 *(21.60-32.40)*	0.7896*	0.8614
	80% ± 15%	23	26.04 ± 1.63 *(21.70-28.90)*	26.23 ± 1.78 *(21.50-29.80)*	0.2933	0.8614
	100% steady-state	23		26.57 ± 1.60 *(23.40-30.30)*	n/a	
494 mmHg	21% steady-state	23		22.88 ± 1.47 *(19.80-26.80)*	n/a	
	35% ± 15%	23	24.01 ± 1.76 *(20.20-27.40)*	23.82 ± 1.59 *(20.60-27.20)*	0.2407	0.8614
	50% ± 15%	23	24.29 ± 1.34 *(21.80-26.70)*	24.41 ± 1.64 *(21.90-27.90)*	0.5067	0.8614
	65% ± 15%	23	24.83 ± 1.50 *(21.70-27.40)*	24.90 ± 1.73 *(21.90-28.00)*	0.6581	0.8614
	80% ± 15%	23	25.19 ± 1.73 *(21.70-28.80)*	25.19 ± 1.79 *(22.10-28.60)*	0.9858	0.9858
	100% steady-state	23		25.56 ± 1.57 *(22.80-28.10)*	n/a	

Supplemental Table 4: Arterial Blood SaO2 Comparisons. Supplemental Table 4 presents arterial blood sample SaO_2 values measured immediately upon reaching the predetermined F_iO_2 level (following the final non-steady-state exposure) with those measured 120 seconds later during steady-state F_iO_2. Comparisons were performed using paired *t*-tests unless otherwise indicated. †Sample size decreased as a result of one participant whose arterial line catheter became non-functional during the latter part of the experimental protocol.
[*] *p*-value from Wilcoxon Signed Rank test; Adj. *p*-values from false discovery rate (FDR).

	F_iO_2 range during non-steady state/steady state hyperoxia exposure	**N†**	**SaO_2 Measured upon reaching predetermined F_iO_2 level following non-steady state/steady state hyperoxia exposure** (Mean ± SD) *Range*	**SaO_2 Measured after maintaining predetermined F_iO_2 level for 120 seconds** (Mean ± SD) *Range*	***p*-value[*]**	**Adj. *p*-value**
749 mmHg	21% steady-state	24		97.29 ± 1.12 *(94.00-99.00)*	n/a	
	35% ± 15%	24	99.96 ± 0.20 *(99.00-100.00)*	99.71 ± 0.69 *(97.00-100.00)*	0.0625	0.0938
	50% ± 15%	24	99.96 ± 0.20 *(99.00-100.00)*	99.96 ± 0.20 *(99.00-100.00)*	---	
	65% ± 15%	24	100.00 ± 0.00 *(100.00-100.00)*	100.00 ± 0.00 *(100.00-100.00)*	---	
	80% ± 15%	24	100.00 ± 0.00 *(100.00-100.00)*	100.00 ± 0.00 *(100.00-100.00)*	---	
	100% steady-state	24		100.00 ± 0.00 *(100.00-100.00)*	n/a	
565 mmHg	21% steady-state	24		93.38 ± 2.18 *(86.00-97.00)*	n/a	
	35% ± 15%	24	99.21 ± 0.51 *(98.00-100.00)*	98.63 ± 0.77 *(63.00-100.00)*	0.0002[*]	0.0006
	50% ± 15%	24	99.92 ± 0.28 *(99.00-100.00)*	99.54 ± 1.06 *(95.00-100.00)*	0.0313[*]	0.0563
	65% ± 15%	23	100.00 ± 0.00 *(100.00-100.00)*	99.96 ± 0.21 *(99.00-100.00)*	1.0000	1.0000
	80% ± 15%	23	100.00 ± 0.00 *(100.00-100.00)*	100.96 ± 0.21 *(99.00-100.00)*	1.0000	1.0000
	100% steady-state	23		100.00 ± 0.00 *(100.00-100.00)*	n/a	
494 mmHg	21% steady-state	23		84.42 ± 4.34 *(73.00-92.00)*	n/a	
	35% ± 15%	23	97.96 ± 1.00 *(95.00-99.00)*	95.04 ± 2.55 *(87.00-98.00)*	<.0001[*]	0.0005
	50% ± 15%	23	99.26 ± 0.69 *(97.00-100.00)*	98.65 ± 0.78 *(96.00-99.00)*	0.0002[*]	0.0006
	65% ± 15%	23	99.87 ± 0.46 *(98.00-100.00)*	99.61 ± 0.72 *(97.00-100.00)*	0.0313[*]	0.0563
	80% ± 15%	23	100.00 ± 0.00 *(100.00-100.00)*	99.91 ± 0.42 *(98.00-100.00)*	1.0000	1.0000
	100% steady-state	23		100.00 ± 0.00 *(100.00-100.00)*	n/a	

Supplemental Table 5: Arterial Blood Glucose Comparisons. Supplemental Table 5 presents arterial blood sample glucose values measured immediately upon reaching the predetermined F_iO_2 level (following the final non-steady-state exposure) with those measured 120 seconds later during steady-state F_iO_2. No significant differences were found. Comparisons were performed using paired *t*-tests unless otherwise indicated. †Sample size decreased as a result of one participant whose arterial line catheter became non-functional during the latter part of the experimental protocol. [*] *p*-value from Wilcoxon Signed Rank test. Adj. *p*-values from false discovery rate (FDR).

	F_iO_2 range during non-steady state/steady state hyperoxia exposure	**N†**	**Glucose Measured upon reaching predetermined F_iO_2 level following non-steady state/steady state hyperoxia exposure** (Mean ± SD) *Range*	**Glucose Measured after maintaining predetermined F_iO_2 level for 120 seconds** (Mean ± SD) *Range*	***p*-value**	**Adj. *p*-value**
749 mmHg	21% steady-state	24		100.83 ± 11.36 *(84.00-129.00)*	n/a	
	35% ± 15%	24	104.08 ± 14.33 *(87.00-148.00)*	103.13 ± 13.34 *(87.00-142.00)*	0.1383	0.4149
	50% ± 15%	24	103.25 ± 14.18 *(87.00-143.00)*	103.71 ± 14.21 *(84.00-143.00)*	0.5156	0.6997
	65% ± 15%	24	102.25 ± 13.34 *(85.00-138.00)*	102.75 ± 12.86 *(86.00-137.00)*	0.3537	0.6063
	80% ± 15%	24	102.67 ± 12.27 *(85.00-135.00)*	101.96 ± 11.82 *(84.00-133.00)*	0.0985	0.4149
	100% steady-state	24		102.21 ± 11.22 *(85.00-133.00)*	n/a	
565 mmHg	21% steady-state	24		100.08 ± 10.76 *(83.00-128.00)*	n/a	
	35% ± 15%	24	99.96 ± 10.58 *(85.00-119.00)*	100.83 ± 10.81 *(84.00-121.00)*	0.0673	0.4149
	50% ± 15%	24	101.71 ± 11.57 *(81.00-132.00)*	101.50 ± 11.08 *(85.00-128.00)*	0.6026	0.7231
	65% ± 15%	23	100.48 ± 11.73 *(83.00-131.00)*	100.43 ± 11.58 *(84.00-127.00)*	0.8981	0.8981
	80% ± 15%	23	100.30 ± 10.83 *(82.00-127.00)*	100.61 ± 10.16 *(83.00-127.00)*	0.3282	0.6063
	100% steady-state	23		99.75 ± 9.97 *(80.00-124.00)*	n/a	
494 mmHg	21% steady-state	23		97.79 ± 8.85 *(82.00-115.00)*	n/a	
	35% ± 15%	23	96.78 ± 8.98 *(82.00-118.00)*	97.30 ± 9.33 *(80.00-117.00)*	0.1739	0.4174
	50% ± 15%	23	99.13 ± 8.42 *(84.00-117.00)*	99.70 ± 8.57 *(85.00-119.00)*	0.1196	0.4149
	65% ± 15%	23	99.87 ± 8.55 *(85.00-119.00)*	99.83 ± 8.51 *(84.00-121.00)*	0.8701	0.8981
	80% ± 15%	23	98.87 ± 8.65 *(85.00-124.00)*	99.13 ± 8.01 *(82.00-119.00)*	0.5248	0.6997
	100% steady-state	23		98.78 ± 8.53 *(83.00-121.00)*	n/a	

Supplemental Table 6: Arterial Blood Hematocrit Comparisons. Supplemental Table 6 presents arterial blood sample hematocrit values measured immediately upon reaching the predetermined F_iO_2 level (following the final non-steady-state exposure) with those measured 120 seconds later during steady-state F_iO_2. Comparisons were performed using paired *t*-tests unless otherwise indicated.
†Sample size decreased as a result of one participant whose arterial line catheter became non-functional during the latter part of the experimental protocol.
[*] *p*-value from Wilcoxon Signed Rank test; Adj. *p*-values from false discovery rate (FDR).

	F_iO_2 range during non-steady state/steady state hyperoxia exposure	**N†**	**Hematocrit Measured upon reaching predetermined F_iO_2 level following non-steady state/steady state hyperoxia exposure** (Mean ± SD) *Range*	**Hematocrit Measured after maintaining predetermined F_iO_2 level for 120 seconds** (Mean ± SD) *Range*	***p*-value**	**Adj. *p*-value**
749 mmHg	21% steady-state	24		41.54 ± 2.98 *(35.00-46.00)*	n/a	
	35% ± 15%	24	41.71 ± 3.13 *(35.00-46.00)*	41.54 ± 3.04 *(35.00-46.00)*	0.5596	0.6451
	50% ± 15%	24	41.13 ± 3.42 *(34.00-46.00)*	41.88 ± 3.04 *(35.00-47.00)*	0.0098[*]	0.1176
	65% ± 15%	24	41.46 ± 3.32 *(34.00-47.00)*	41.75 ± 3.07 *(35.00-46.00)*	0.1431	0.5724
	80% ± 15%	24	41.75 ± 2.95 *(35.00-46.00)*	41.58 ± 3.16 *(35.00-46.00)*	0.2891	0.6451
	100% steady-state	24		41.50 ± 3.18 *(34.00-46.00)*	n/a	
565 mmHg	21% steady-state	24		41.88 ± 3.21 *(35.00-47.00)*	n/a	
	35% ± 15%	24	42.00 ± 3.23 *(35.00-47.00)*	42.08 ± 3.08 *(36.00-47.00)*	0.5913	0.6451
	50% ± 15%	24	41.67 ± 3.14 *(35.00-46.00)*	42.00 ± 3.01 *(35.00-46.00)*	0.0781	0.4686
	65% ± 15%	23	41.87 ± 3.20 *(34.00-47.00)*	42.00 ± 3.15 *(35.00-47.00)*	0.4551	0.6451
	80% ± 15%	23	41.78 ± 3.01 *(35.00-46.00)*	41.91 ± 3.23 *(34.00-47.00)*	0.5625	0.6451
	100% steady-state	23		42.08 ± 3.27 *(35.00-47.00)*	n/a	
494 mmHg	21% steady-state	23		42.08 ± 3.20 *(35.00-47.00)*	n/a	
	35% ± 15%	23	42.13 ± 3.24 *(35.00-47.00)*	42.30 ± 3.31 *(35.00-47.00)*	0.3438	0.6451
	50% ± 15%	23	42.04 ± 3.48 *(34.00-47.00)*	42.09 ± 3.38 *(34.00-47.00)*	1.0000	1.0000
	65% ± 15%	23	42.09 ± 3.42 *(34.00-48.00)*	42.26 ± 3.12 *(35.00-47.00)*	0.3984	0.6451
	80% ± 15%	23	41.91 ± 3.41 *(34.00-47.00)*	42.13 ± 3.28 *(35.00-47.00)*	0.3398	0.6451
	100% steady-state	23		42.22 ± 3.26 *(35.00-47.00)*	n/a	

LIST OF SYMBOLS, ABBREVIATIONS AND ACRONYMS

ABG	Arterial blood gas
BE	Base excess
BMI	Body Mass Index
CNS	Central nervous system
cmH_2O	Centimeters of water
CO_2	Carbon dioxide
COVID	Coronavirus disease
CRP	C-reactive protein
ELISA	Enzyme-linked immunosorbent assay
FDR	False discovery rate
ft	Feet
F_iO_2	Fraction of inspired oxygen
Flt-1	Vascular endothelial growth factor receptor 1
fNIRS	Functional Near Infrared Spectroscopy
GLM	General Linear Model
HCO_3-	Bicarbonate ion
HRF	Hemodynamic response function
ICAM-1	Intercellular adhesion molecule-1
IFN-γ	Interferon-gamma
IL-2	Interleukin 2
IL-4	Interleukin 4
IL-5	Interleukin 5
IL-6	Interleukin 6
IL-7	Interleukin 7
IL-8	Interleukin 8
IL-10	Interleukin 10
IL-12	Interleukin 12
IL-13	Interleukin 13
IL-15	Interleukin 15
IL-16	Interleukin 16
IL-17A	Interleukin 17A
IL-1α	Interleukin 1 alpha
IL-1β	Interleukin 1 beta
IP-10	Interferon γ-induced protein 10,000 Dalton (10 kDa)
MCP-1	Monocyte chemoattractant protein-1
MCP-4	Monocyte chemoattractant protein-4
MDC	Macrophage-derived chemokine
MIP-1α	Macrophage inflammatory protein-1 alpha
MIP-1β	Macrophage inflammatory protein-1 beta
m	Meters
mmHg	Millimeters of mercury
mL	Milliliters
mL/min/100g	Milliliters per minute per 100 grams
O_2	Oxygen
OBOGs	Onboard oxygen generation systems
PaO_2	Partial pressure of arterial blood oxygen

$PaCO_2$	Partial pressure of carbon dioxide
pH	Potential of hydrogen
PlGF	Placental growth factor
SAA	Serum amyloid A
SaO_2	Arterial blood oxygen saturation
SAS	Statistical Analysis Software
SD	Standard deviation
TARC	Thymus activation regulated chemokine
TCO_2	Total carbon dioxide content
Tie-2	Tyrosine kinase 2
TNF-α	Tumor necrosis factor alpha
TNF-β	Tumor necrosis factor beta
VCAM-1	Vascular cell adhesion molecule-1
VEGF-A	Vascular endothelial growth factor A
VEGF-C	Vascular endothelial growth factor C
VEGF-D	Vascular endothelial growth factor D
%	Percent